Verification of precipitation calculation method based on parameterization of distribution function evolution.

I.V.Akimov
Hydrometeorological Centre of Russia
11-13 Bolshoy Predtechensky per., 123242, Moscow-242, Russia.
E-mail: akimov@rhmc.mecom.ru

The new precipitation calculation method presented in [1] was evaluated. The method is based on different approach, than used in Kessler-type parameterizations. In Kessler approach [2] the precipitation beginning from cloudy layer is permitted after cloud water content reaches some value, named as autoconversion threshold. But the value of this threshold could not be obtained from the measurements and the hypothesis about such threshold contradicts with the observed facts that precipitation starts from clouds when cloud water content rises up to quite different values [3,4]. Therefore the new method is based on consideration of precipitation beginning process as formation of part of cloud spectra consisting of large drops which falls out as a precipitation. This is realized by parametric description distribution function evolution during precipitation formation process. The main processes that influence on distribution function evolution are gravitational and turbulent coalescence in liquid clouds and sublimation of water vapour on ice crystals in mixed phase clouds.

The proposed method was included as precipitation parameterization module in global spectral model of the Hydrometcentre of Russia T85L31. The precipitation calculation module that was used in old version of model is based on Kessler parameterization. Therefore the comparison of precipitation fields obtained from new version of model with results obtained from old version allows to evaluate the distinction between two different parameterization approaches. Two scores were chosen for verification analysis. The accuracy of precipitation spatial distribution forecast was characterized by Pearcy-Obychov criterion T (also known as Hanssen and Kuipers discriminant). The value of this score vary from T=1 for ideal forecast to T=-1 for absolutely incorrect forecast. The accuracy of precipitation quantity calculation was characterized by root-mean-square error σ_Q.

The evaluation of precipitation forecasts obtained from two versions of model was conducted during time period March-December 2002. The values of T and σ_Q scores are presented on the figure. The estimation was performed using precipitation observation data from four regions in northern hemisphere. Figure shows that T criterion values resulted from new model version precipitation forecast is greater during all estimations period than values obtained from old model version integration. So for European part of Russia in period April-July criterion T value rises from level 0.2-0.3 to level 0.3-0.5. The usage of new precipitation calculation method also reduces forecast error σ_Q in all regions except North America. The values σ_Q is became smaller on 10-20% in comparison with errors resulted from old version of model. In North America at time period June-August the new version of model gives σ_Q values that overcame error level of old model version. The reason of this fact that new precipitation calculation method uses empirical relations and values of parameters, which were obtained from aircraft measurements data performed in middle latitudes region. But the weather conditions in south coast of North America in summer season is close to tropical weather. Therefore the usage of such parameters in this season is not quite correct. The possible way to eliminate this is to select different values of parameters included in new method for different climatic regions. In common figure shows that incorporation of new method in global spectral atmospheric model resulted in improvement of precipitation forecast in midlatitude region.

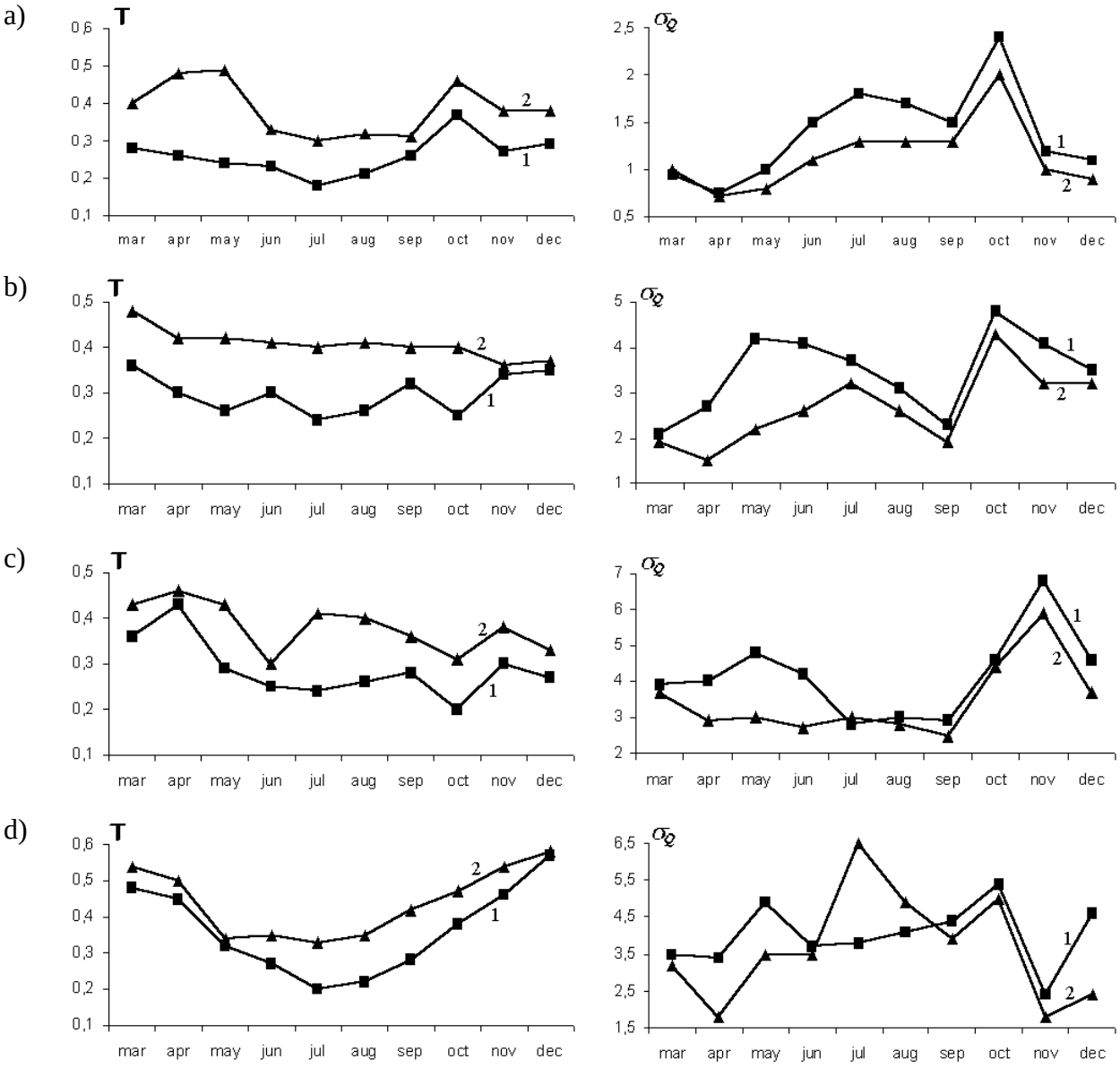

Pearcy-Obychov criterion T and forecast root-mean square error σ_Q for 24 hours precipitation forecast, calculated for verification period March - December 2002. Versions of model: 1- old version, 2- version including new method of precipitation calculation. Regions of estimations: European part of Russia (a), Central Europe (b), West Europe (c), North America (d).

References:

1. Akimov I.V., 2003. Method of precipitation intensity calculation based on microphysical processes parameterization in liquid and mixed phase clouds. Izvestia. Atmospheric and oceanic physics. v. 39.

2. Kessler E., 1969. On the distribution and continuity of water substance in atmospheric circulations. Meteor. Monogr., vol. 10.

3. Matveev L.T., 2000. Physics of atmosphere. S.Pb. Hydrometeoizdat.

4. Mason B.J., 1971. The physics of clouds. Clarendon Press, Oxford.

A Prognostic Cloud Ice Scheme for NWP-Models

G. Doms, D. Majewski, A. Müller and B. Ritter
Deutscher Wetterdienst, P.O.Box 100465, 63004 Offenbach a.M., Germany
e-mail: guenther.doms@dwd.de, detlev.majewski@dwd.de, aurelia.mueller@dwd.de, bodo.ritter@dwd.de

Most grid-scale cloud schemes used in NWP-models solve only one prognostic equation for cloud condensate. Hence, the distinction of the water and the ice phase has to be determined diagnostically for temperatures below the freezing point $T_0 = 0°C$. This is usually done by (i) prescribing the liquid fraction in the total condensate as a function f_l of temperature and (ii) assuming that both cloud ice and cloud water are in thermodynamic equilibrium with respect to a hypothetical saturation vapour pressure given by $e_s = f_l\, e_s^w + (1 - f_l)\, e_s^i$, where e_s^w and e_v^i are the saturation vapour pressure over water and ice, respectively. The function f_l for the liquid fraction is usually chosen to be 1 for $T > T_0$ and 0 for temperatures below a threshold T_{ice} with a linear or quadratic decrease with temperature in the range $T_{ice} < T < T_0$. Various values $-40°C < T_{ice} < -10°C$ are assumed in different schemes.

A class of cloud schemes simply neglects the cloud ice phase ($f_l = 1$ for all temperatures) as for instance done in the operational schemes of the global model GME and the regional model LM of DWD. This strategy, however, results in a wrong thermodynamic state of cirrus clouds (always water clouds at water saturation) with corresponding errors the cloud-radiation feedback, and in a large positive bias of upper-level humidity. On the other hand, ice-schemes with a prescribed temperature dependent liquid fraction have also a number of conceptional drawbacks. First, the assumption of thermodynamic equilibrium of both water and ice at temperatures below T_0 is not in accordance with physical principles. Second, for $T < T_{ice}$ a saturation adjustment is done for the calculation of condensate; since the number of cloud ice crystals is very small, such an instantaneous adjustment has no physical basis. Third, effects from the Bergeron-Findeisen process cannot be considered explicitly, since the ice-phase is in thermodynamic equilibrium. Fourth, the Seeder-Feeder mechanism is not represented: deep clouds are more likely to be glaciated than thin clouds at the same temperature. And fifth, ice falling from above into sub-freezing layers is forced to melt in order to maintain the prescribed liquid fraction – this is not very realistic.

Bearing in mind these difficulties, a new parameterization scheme was designed to take into account cloud ice and cloud water by a separate prognostic budget equations. As a novel feature of the scheme, we formulate the depositional growth of cloud ice as a non-equilibrium process and require, at all temperatures, saturation with respect to water for cloud liquid water to exist. The explicit calculation of cloud ice depositional growth is based on the mass-growth equation of single pristine crystals. By prescribing cloud ice particles as thin hexagonal plates with a monodispers size distribution, the total growth rate of cloud ice mixing ration q_i due to deposition (sublimation) may then be derived as

$$(\dot{q}_i)_{dep} \;=\; c_i\,(N_i)^{2/3}\,(\rho q_i)^{1/3}\,q_v^{si}(\,S_i - 1,\,) \tag{1}$$

in terms of the ice-supersaturation (subsaturation) $S_i = q_v/q_v^{si}$, where q_v is the specific humidity and q_v^{si} is its saturation value over the ice. c_i is a slowly varying function of temperature and pressure, which is approximated by a constant value of of $1.5 \cdot 10^{-5}$ (in corresponding SI-units). The number density $N_i(T)$ of cloud-ice particles is parameterized as a function of air temperature using the relation $N_i(T) = N_0^i \exp\{\,0.2\,(T_0 - T)\}$ with $N_0^i = 1.0 \cdot 10^2 m^{-3}$, which is an empirical fit to available data from aircraft measurements in stratiform clouds. Cloud ice is initially formed by heterogeneous nucleation or homogeneous freezing of supercooled droplets. The latter process is parameterized by instantaneous freezing of cloud water for temperatures below $-37°C$. For heterogeneous nucleation, we simply assume that $N_i(T)$ ice forming nuclei with a very small initial mass are activated within a time step and that the temperature is below a nucleation threshold (set to $-7°C$). According to results from field experiments, we require water saturation for the onset of cloud ice formation above a temperature threshold T_d (set to $-25°C$). For temperatures below T_d, deposition nucleation may occur for any ice supersaturation. All other conversion rates are parameterized in a similar way as in standard cloud microphysics schemes.

Ice crystals which nucleate in a water saturated environment will grow very quickly by vapour deposition due to a high ice supersaturation S_i according to (1). Depending on local thermodynamic conditions, the existing cloud water will either evaporate completely, or will be resupplied by condensation. The first

case is expected for weak dynamical forcings, where the initial mixed-phase cloud will rapidly glaciate to become an ice cloud existing at or near ice saturation. The second case is expected for strong dynamical forcings along fronts or in the vicinity of convection, where water saturation with mixed phase clouds can be maintained. Thus, the liquid fraction will physically adjust and an empirical specification is not required. Moreover, precipitation enhancement mechanisms such as the Bergeron-Findeisen or the Seeder Feeder process are represented explicitly and additional parameterizations are avoided.

A first tentative validation with the global model GME running in 'climate' mode revealed that the inclusion of cloud ice greatly improves the outgoing longwave radiation due to different radiative properties of cloud ice compared to cloud water. Meanwhile, a parallel test suite including data assimilation has been established. First verification results show slightly improved scores for 2m-temperature and 500 hPa geopotential height correlation, and a better representation of the upper-level humidity and cloud structures. As an example, Figure 1 compares the relative humidity over water at 250 and 500 hPa resulting from 24-h GME runs with the operational and with the cloud-ice scheme. At the 250 hPa level, the routine scheme results in unrealistic high humidities close to water saturation in equatorial and mid-latitude regions associated with tropical convection and frontal systems, respectively. With the cloud-ice scheme, the relative humidity is significantly reduced in these regions – down to values around 60-70%, which indicate ice-saturation. Only for a few gridpoints in tropical regions or along frontal clouds mixed-phase at water saturation are simulated. At the warmer 500 hPa level, the spatial distribution of relative humidity from the two forecasts is very similar – except for cold high latitude regions, where cloud-ice scheme again results in a drastic reduction of relative humidity.

Given a successful completion of the test suite, an operational introduction of the cloud-ice scheme is scheduled for May 2003. At the same time, the new scheme will also be switched on in the regional model LM as well as in LMs at MeteoSwiss (Switzerland), ARPA-SMR (Italy), HNMS (Greece) and IMGW (Poland), and in ten HRMs running world wide.

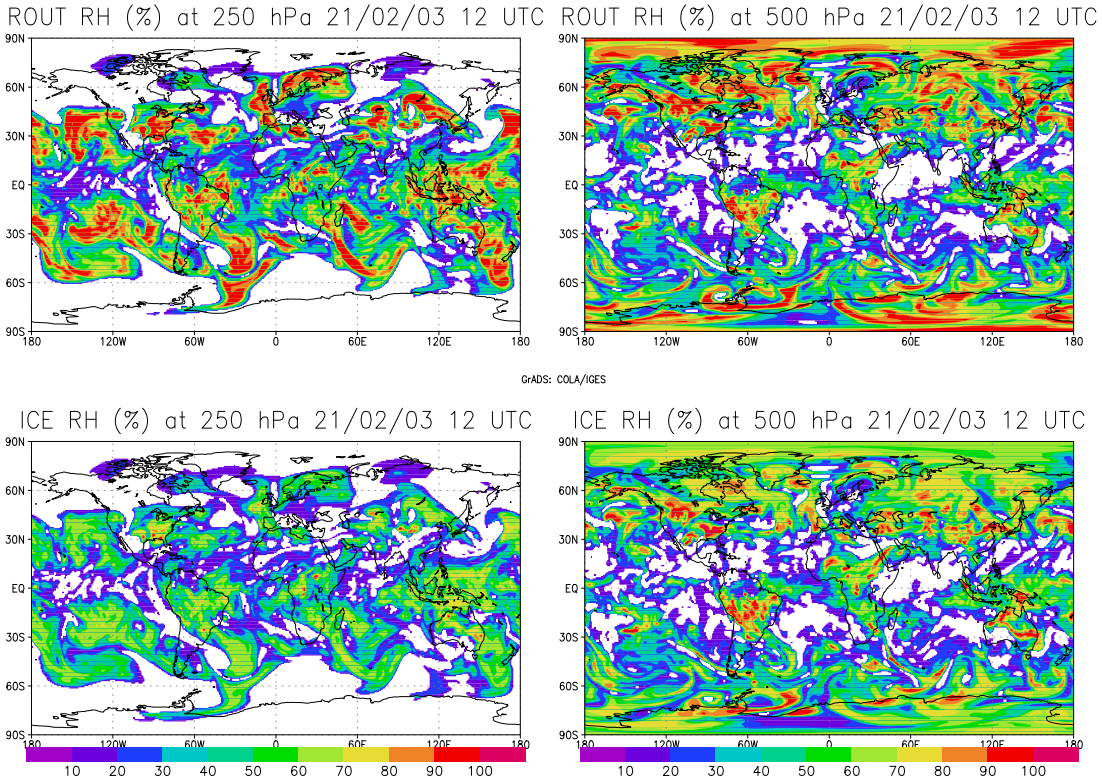

Figure 1: Relative humidity at 250 hPa (left) and 500 hPa (right) for theoperational cloud scheme (top) and the new cloud-ice scheme (bottom). 24-h GME forecasts starting from 20 February 2003 12 UTC.

The SNOWMIP project : validation of albedo and short wave radiation budget simulated by several snow models.

P. Etchevers[1], E. Martin[1], R. Brown[2], C. Fierz[3],Y. Lejeune[1]E. Bazile[4], A. Boone[4], Y.-J. Dai[5], R. Essery[6], A. Fernandez[7] , Y. Gusev[8], R. Jordan[9], V. Koren[10] , E. Kowalczyk[11], N. O. Nasonova[8], R. D. Pyles[12], A. Schlosser[13], A. B.Shmakin[14], T. G. Smirnova[15], U. Strasser[16], D. Verseghy[2], T. Yamazaki[17], Z.-L. Yang[18]

[1]Centre d'Etudes de la Neige, CNRM /Météo-France, Grenoble, France [2]Canadian Meteorological Service, Dorval, Qc, Canada [3]Swiss Federal Institute for Snow and Avalanche Research (SLF), Flüelastrasse 11, CH-7260 Davos Dorf, Switzerland [4]Météo-France, CNRM, Toulouse, France, [5]Institute of Atmospheric Physics; Chinese Academy of Sciences, Beijing, China, [6]Met Office, Bracknell, Berks. U.K., [7]Instituto Nacional de Meteorologia, Madrid, Spain, [8]Laboratory of Soil Water Physics, Institute of Water Problems, Russian Academy of Sciences, Moscow, Russia, [9]CRREL, Cold Regions Research and Engineering Laboratory,Hanover, U.S.A., [10]NOAA/NWS/OH1/HRL, Silver Spring, MD 20910 U.S.A., [11]CSIRO Atmospheric Research, Aspendale, Australia, [12]Cooperative Institute for Research in the Environmental Sciences, Boulder, U.S.A., [13]COLA/IGES, Calverton, U.S.A., [14]Laboratory of Climatology, Institute of Geography, Russian Academy of Sciences, Moscow, Russia, [15]Forecast Systems Laboratory, Boulder, USA, [16]Institute of Hydromechanics and Water Resources Management; ETH-Hönggerberg, Zürich, Switzerland, [17]Frontier Observational Research System for Global Change, Tohoku University, Sendai, Japan, [18]Dept of Hydrology and Water Resources, The University of Arizona, Tucson, U.S.A.

Email : snowmip@meteo.fr

Introduction

Over the last thirty years, many snow models have been developed and have been used for various applications such as hydrology, global circulation models, snow monitoring, snow physics and avalanche forecasting. The degree of complexity of these models is highly variable, from simple index methods to multi-layer models simulating snow cover stratigraphy and texture.

In the project SnowMIP (www.cnrm.meteo.fr/snowmip/), four sites were chosen for the comparison of the snow models. As albedo and snow surface temperature measurement are not available for all of them, only the Col de Porte (CDP) and Weissfluhjoch (WFJ) data are used in this paper. The Col de Porte is a middle elevation site located in the French Alps (1340 m). Weissfluhjoch is a more mountainous site that lies at an altitude of 2500 m in the Swiss Alps.

Albedo parametrization

The incoming short wave radiation is the same for all the models and the short wave radiation budget simulation depends on the fraction of the radiation which is reflected by the snowpack, i.e. the snow albedo. The albedo parametrizations of the 23 models are based on temperature (6 models), snow types and/or grain size (6 models), or age (13 models). Four models use either no albedo or a fixed albedo (index based, or a constant albedo, or an albedo depending only on vegetation fraction or shading). Some models use two parameterisations, e.g. age can account for all the aging processes of snow or can be used in conjunction with a parameterisation based on snow grain size or type.

The albedo increases are generally determined by snowfalls. The albedo decreases are more complex because they depend on the snow micro-structure and grain types. As stated above, the decrease of albedo is generally calculated by the models as a function of the snow age, surface temperature, grain size and other parameters provided by the model itself. These parametrizations play a major role in the model performances because albedo is a key factor for calculating the snowmelt. Thus, it appears interesting to examine the accuracy of parametrizations for some particular periods. These selected periods cover at least eight days and do not include snow fall events (table 1). The three CDP periods correspond to snowmelt events and the albedo decrease (-1.63×10^{-2} per day on average) is due to the appearance of liquid water in the snowpack. At WFJ, the decrease is 5 times weaker (-3.17×10^{-3} per day on average) because it is due to dry snow evolution (without melting or rain). The quality of each simulation is estimated by comparing the change in observed and simulated albedos between the beginning and end of each period. The albedo decrease averaged for all models is pretty accurate for all the episodes (table 1), but the extreme values show that some models are far from the reality. For the 6 episodes, the rms error of the albedo variation ranges from 0.07 to 0.13, but average results are very different for the two sites.

	Site	Period	Number of days	Observed albedo (beginning and end)	Observed albedo variation (per day)	Simulated albedo variations: average (per day)	Simulated albedo variations: min-max (per day)
Episode 1	CDP9697	28/02/97-14/03/97	15	0.63-0.5	-0.0087	-0.01	-0.02/0.005
Episode 2	CDP9798	24/01/98-20/02/98	28	0.77-0.59	-0.0064	-0.006	-0.01/0.001
Episode 3	CDP9798	19/04/98-26/04/98	8	0.8-0.53	-0.0338	-0.015	-0.03/0.00
Episode 4	WFJ	13/12/92-02/01/93	21	0.9-0.86	-0.0019	-0.005	-0.01/0.005
Episode 5	WFJ	29/01/03-14/02/93	17	0.91-0.8	-0.0065	-0.008	-0.02/0.00
Episode 6	WFJ	21/04/93-29/04/93	9	0.75-0.74	-0.0011	-0.009	-0.03/0.009

Table 1 : The six periods selected to validate albedo decreases. No precipitation occurred during these episodes. The two last columns contain the average for all models and the minimum/maximum values of the simulated albedo variations.

Particular episodes

The rms error is generally larger for the CDP site (0.08 to 0.16) than for the WFJ site (0.03 to 0.11). The performance of a given model depends a lot on its albedo parametrization. For the CDP site, the best models use parametrizations based on the snow age and/or the snow type. As the albedo regularly decreases during the episodes, the age parametrization is adequate to correctly simulate this evolution. This is illustrated by figure 1, where the daily simulated and observed albedos are plotted for episode 3 (CDP9798): many models properly reproduce the albedo decrease from 0.8 to 0.65. Most of these models use a parametrization based on the snow grain size or the snow age. On the contrary, the less accurate models generally include a parametrization using the snow surface temperature. As this parameter does not vary a lot during the melting period, this is not an accurate predictor for the albedo decrease. Finally, if one considers the whole set of episodes, three of the four best models use albedo parametrizations based on snow grain characteristics and snow age. They are able to simulate both the slow albedo decrease in winter and the fast decrease during the melting period. The other models are generally able to simulate properly the albedo for one type of episode but not the other. Only one model using a parametrization based only on the snow age and surface temperature succeeds in simulating the different albedo evolutions.

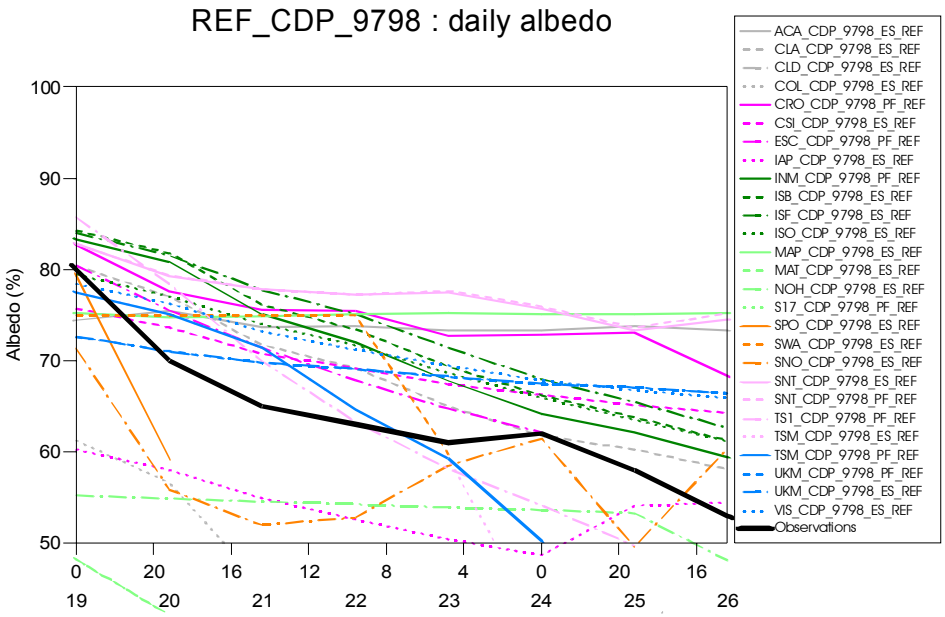

Figure 1 : daily albedo observed (large black line) for episode 3 (CDP site, from 19 to 25 April 1998) The other coloured lines correspond to the 26 albedo simulations.

Development of a New Land-surface Model for JMA-GSM

Masayuki Hirai

Numerical Prediction Division, Japan Meteorological Agency (e-mail:m-hirai@met.kishou.go.jp)

Mitsuo Oh'izumi

Meteorological Research Institute, Japan Meteorological Agency (e-mail: mohizumi@mri-jma.go.jp)

In 1989, a SiB (Simple Biosphere) model was developed as a land-surface scheme for JMA's operational global NWP model (JMA-GSM). However, the SiB model has not been modified substantially after that. Recently, problems considered to be relevant to the land-surface process were pointed out as follows:

* Snow-melting is overestimated in spring. In the Northern Hemisphere, the southern edge of the snow cover area retreats faster comparing with an analysis or observations.
* Warming bias in the lower troposphere on ice sheet area in summer.

In order to solve such problems, we have developed a new land-surface model, which treats soil and snow processes more accurately. Major changes are as follows:

* A conventional force restore method for predicting soil temperature is abandoned and heat conductivity among multiplied soil layers is explicitly calculated.
* Phase change of soil water is considered.
* Multiplied snow layers are introduced and phase change of snow water is considered.
* Snow cover is classified into two categories, "partial snow cover" and "full snow cover".
* A sophisticated snow process is introduced. (Aging of snow albedo, temporal changes of snow density and heat conductivity, keeping water in snow layers and so on.)

We carried out preliminary forecast experiments for April 2002 with JMA-GSM T213L40. Initial condition of soil water for the experiments is set to a model-climate state obtained from a long-term integration of the model, while the operational SiB uses a climate state by Willmott et al. (1985).

The snow cover area for 72 hour forecast (FT72) initiated at 12 UTC April 15, 2002 (validtime is 12UTC April 18, 2002) is shown in Fig. 1. A snow cover area at the Tibetan Plateau is well predicted by the new land-surface model, while not by the operational one. Comparing with the snow cover area estimated from the brightness temperature of SSM/I (See Fig. 2.), the new land-surface model simulates better than the operational one in this region.

Time series of forecast results of sensible and latent heat fluxes and snow depth at a point in the Tibetan Plateau (35N, 90E) are shown in Fig. 3. The new land-surface model well simulates that sensible heat flux decreases reasonably after snow cover forms on the day 2. Instead, latent heat flux increases because of snow sublimation. Net short-wave radiation decreases about 150 W/m^2 and net long-wave radiation increases due to snow cover (not shown).

As a result, it is shown that the new land-surface model properly represents snow process. However, southern edge of the snow cover area still retreats faster than an analysis or observations. Moreover, RMSE (Root Mean Square Error) of the temperature at 850 hPa in the Northern Hemisphere is not improved and a distinct negative bias appears by the new land-surface model.

We go on with development of the land-surface model, planing to put it into operation within a few years.

References

JAPAN METEOROLOGICAL AGENCY, 2002: Land-surface processes, *OUTLINE OF THE OPERATIONAL NUMERICAL WEATHER PREDICTION AT THE JAPAN METEOROLOGICAL AGENCY*, 50-52.

Willmott, C. J., C. M. Rowe, and Y. Mintz, 1985: Climatology of the terrestrial seasonal water cycle. *J. Climatology*, **5**, 589-606.

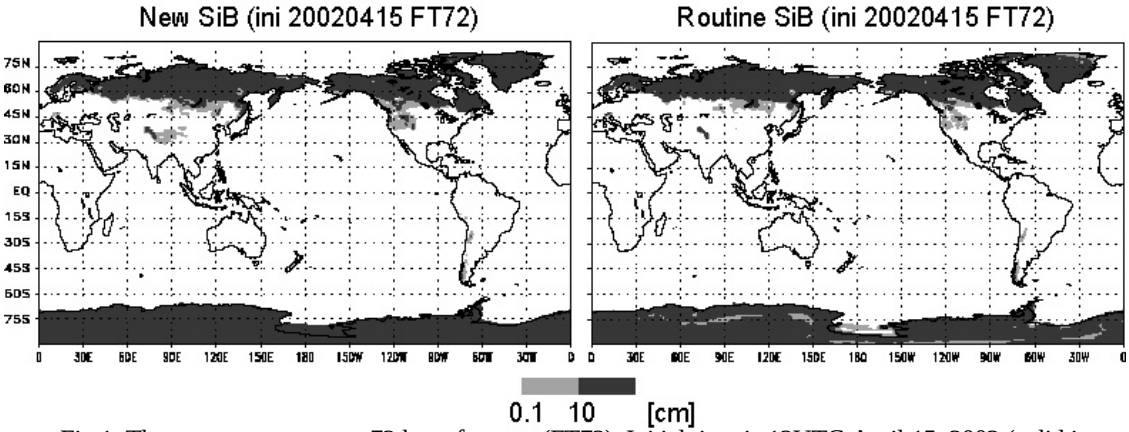

Fig 1. The snow cover area at 72 hour forecast (FT72). Initial time is 12UTC April 15, 2002 (validtime is 12UTC April 18, 2002). The left figure shows a result from the new land-surface model, and right one shows that from the operational one.

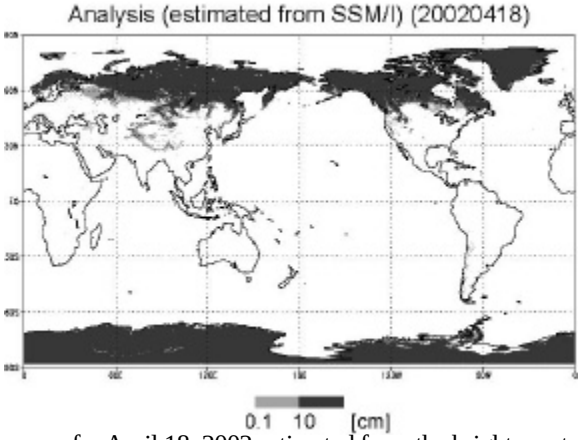

Fig 2. The snow cover area for April 18, 2002 estimated from the brightness temperature of SSM/I.

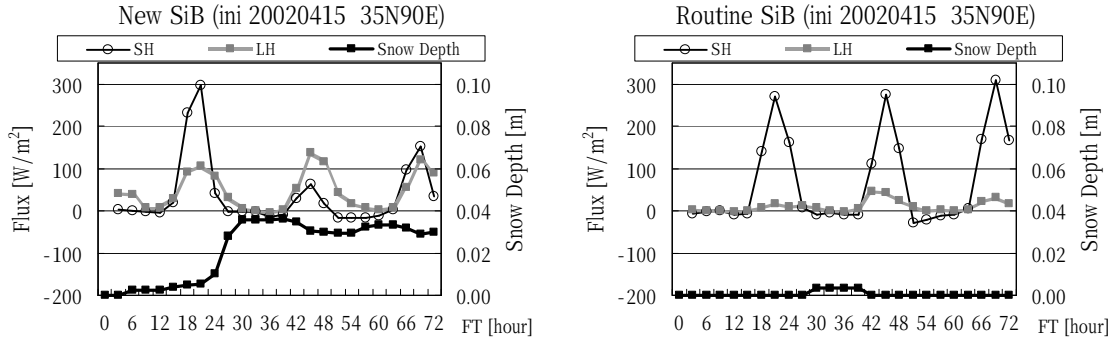

Fig 3. The time series of sensible and latent heat fluxes and snow depth at a point in the Tibetan Plateau (35N, 90E). The result from the new land-surface model is shown in left, and the operational model is in right.

Application of RRTM longwave radiation to NCEP GFS

Y.-T. Hou[1], S. Moorthi, K. Campana, NCEP
and M. Iacono, AER

The longwave (LW) radiative transfer parameterization used in the current NCEP operational Global Forecast System (GFS) atmospheric model was developed at the Geophysical Fluid Dynamics Laboratory (GFDL) (Schwarzkopf and Fels, 1991). Recently, a Rapid Radiative Transfer Model for longwave radiation (RRTM) has been developed at Atmospheric and Environmental Research, Inc. (AER) (Mlawer et al. 1997). The radiative transfer calculation in RRTM is highly accurate with very high computational efficiency, especially in a large model with high vertical resolution. In a 64-layer model test, the RRTM runs in about one half the time as the operational code does. In addition to the major atmospheric absorbing gases included in the operational LW scheme, such as carbon dioxide, water vapor, and ozone, the RRTM also contains numerous minor species such as nitrous oxide, methane, and up to four types of halocarbons. In water vapor continuum absorption calculations, the operational model uses coefficients derived by Roberts et al. (1976), while RRTM uses a more advanced CKD_2.4 model (Clough et al. 1992).

Comparisons of clear-sky cooling rates between the two parameterizations for typical atmospheric profiles show that, in general, differences between the two radiation schemes are relatively small, except in the upper stratosphere, where RRTM produces more cooling effect than the operational LW model. Since December 24, 2002 we have been running a parallel T254-L64 GFS experiment with RRTM. Figure 1 shows comparison of 500 mb geopotential height anomaly correlation scores of 5-day model forecasts between operational model (PP1) and the parallel model (PP2). Zonally averaged 5-day forecast temperature biases (not shown) indicate that RRTM improves tropospheric temperature bias while enhancing the cold bias in the stratosphere. Two five-year climate runs on a T62-L64 model were also conducted for the two LW radiation schemes. Table 1 shows outgoing LW radiation at the top of the model atmosphere (TOA) for the two LW radiation parameterizations and the five-year climatological average from ERBE observations. It shows that the RRTM produces a closer agreement between simulations and observations than the operational model. Comparison of OLR fluxes at the TOA among the two radiation parameterizations and ERBE observation for a five-year average over the months of July and January (not shown) shows that RRTM improves OLR distribution over tropical and summer mid-latitude regions.

Table 1. Five-year averaged monthly OLR (W/m**2) comparisons among the operational LW scheme, the RRTM, and the observations from ERBE data.

Month	Operational-LW	RRTM-LW	ERBE
JAN	241.06	235.90	232.48
APR	242.64	237.45	234.47
JUL	247.89	242.96	239.40
OCT	241.06	235.90	235.30

[1]E-Mail address: yu-tai.hou@noaa.gov

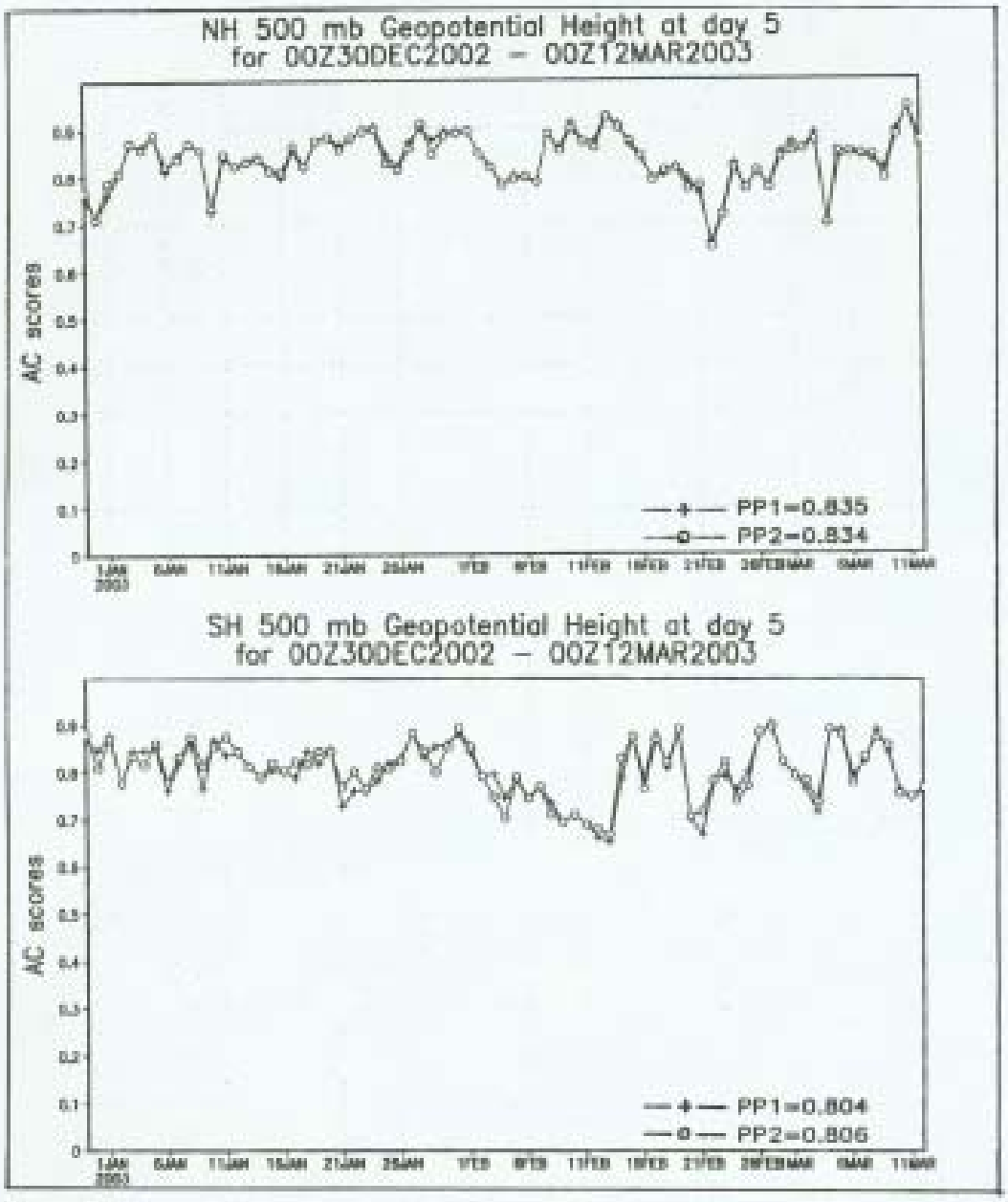

Figure 1. 500-mb geopotential height anomaly correlation scores of 5-day model forecasts. The upper panel is for northern hemisphere and the lower for southern hemisphere.

References:
Clough, S.A., M.J. Iacono, and J.-L.Moncet, 1992, J. Geophys. Res., 97, 15761-15785.
Mlawer, E.J., S.J. Taubman, P.D. Brown, M.J. Iacono, and S.A. Clough, 1997, J. Geophys. Res., 102, 16663-16682.
Roberts, R.E., J.E.A. Selby, and L.M. Biberman, 1976, Appl. Opt., 15, 2085-2090.
Schwarzkopf, M.D., and S.B. Fels, 1991,. J. Geophys. Res., 96, 9075-9096.

Impact of a Cloud Ice Fall Scheme Based on an Analytically Integrated Solution

Hideaki Kawai
Climate Prediction Division, Japan Meteorological Agency
(e-mail: h-kawai@met.kishou.go.jp)

1. Background

Cloud Ice Fall in global NWP model or climate model is very bothersome to treat because the product of the fall speed (v_{ice}) and the time step (Δt) often exceeds the thickness of a vertical layer (Δz) of the model. Since explicit time integration cannot be used practically, the process in our Global Spectral Model (GSM) has been treated as follows:

- In cases $v_{ice}\Delta t \le \Delta z$, cloud ice content ($q_{ice}$) in a layer is distributed into the layer itself and a layer just below the original layer exactly.
- In cases $\Delta z < v_{ice}\Delta t \le 2\Delta z$, a part of cloud ice content is distributed into only a layer just below the original layer exactly and the other part of it falls through into ground surface within a time step.
- In cases $v_{ice}\Delta t > 2\Delta z$, all the cloud ice content falls into ground surface within a time step.

The treatment works appropriately as far as $v_{ice}\Delta t$ is smaller than Δz. Time step in T213 Euler model, which is our operational short-range to 1-week forecast model, meets this condition in almost all cases. But in T106, which is our 1-month forecast model, and in T63, with which we will start 3-month dynamical forecast from March 2003, the condition is not satisfied and a large part of cloud ice falls into ground surface within one time step. Moreover, long time step will become a serious problem for cloud ice fall process in T213 after an adoption of semi-Lagrangian time integration scheme in T213 (T_L319) scheduled in 2003.

2. Scheme based on Analytically Integrated Solution

To avoid the above problem, time integration for cloud ice fall is implemented following analytically integrated solutions below (Rotstayn 1997, Jakob 2000).

$$q_{ice}(t+\Delta t) = q_{ice}(t)e^{-D\Delta t} + \frac{C}{D}(1-e^{-D\Delta t})$$

$$C = \frac{R_f}{r\Delta z} + C_{gnrt}, \qquad D = \frac{a_{<100}v_{ice}}{\Delta z} + \frac{a_{>100}}{\Delta t}$$

where R_f is the cloud ice flux from the above layer, r is the air density, $a_{<100}$ ($a_{>100}$) is the ratio of cloud ice particles whose sizes are smaller (larger) than 100 micrometer. Cloud ice content is separated into two categories following Jakob (2000) and McFarquhar and Heymsfield (1997). Since GSM adopts the cloud distribution concept by Sommeria and Deadorff (1977), cloud water content has been distributed into cloud water (ice) and water vapor at first step (to produce $q_{ice}{}^{*}(t+\Delta t)$) and then, cloud ice fall process has been calculated at second step (to produce $q_{ice}(t+\Delta t)$). But this two-step procedure leads to an unreasonable overestimation of amount of cloud ice fall and consequent lack of cloud ice content. Therefore cloud ice generation rate C_{gnrt}($= (q_{ice}{}^{*}(t+\Delta t) - q_{ice}(t))/\Delta t$) is introduced in order to treat generation and fall of cloud ice simultaneously. This procedure is more correct theoretically and avoids abrupt change of cloud ice content.

3. Result

The results of one-month integration using T63 for December 1988 are shown. Figure 1 shows zonal means of cloud water content (including both the liquid and solid state) of analytical and original schemes. Cloud water content is considerably increased at an

altitude where the state is solid. The increase is preferable because cloud water content of analytical scheme is closer to equilibrium one ($q_{ice}{}^{*}(t+\Delta t)$) provided by the cloud distribution scheme. Fig.2 shows an impact and a current scheme error from Earth Radiation Budget Experiment (ERBE) data on outgoing longwave radiation (OLR). Analytical solution scheme reduces the positive error on OLR to some extent, for example, over Amazon. It has also been confirmed that new scheme improves the overestimation on net downward shortwave radiation at the top of the atmosphere a little bit (not shown). The remaining biases are probably resolved by sophisticated treatments of radiation processes (Kitagawa and Yabu 2002) and by increasing cloud amount based on a review of a probability distribution function in the cloud distribution scheme.

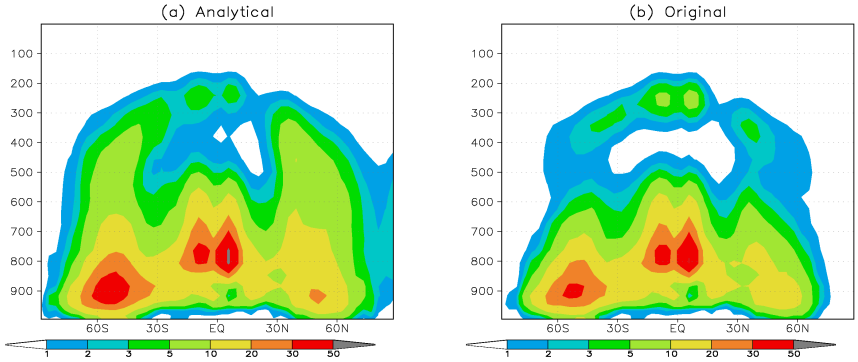

Fig. 1: Zonal means of cloud water content in unit of 10^{-6}[kg/kg] for December 1987 calculated by (a) analytical solution scheme and (b) original scheme. Vertical axis shows pressure [hPa].

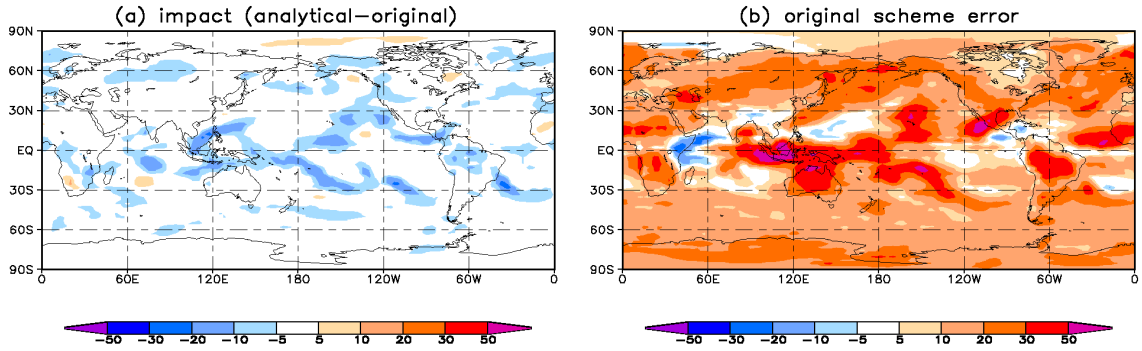

Fig. 2: Outgoing longwave radiation [W/m^2] (a) impact and (b) error for December 1987. Error is calculated based on ERBE observation data.

References

Jakob, C., 2000: The representation of cloud cover in Atmospheric General Circulation Models, ECMWF.

Kitagawa, H., and S. Yabu, 2002: Impact of a revised parameterization of cloud radiative forcings on earth's radiation budgets simulation. Research Activities in Atmospheric and Oceanic Modelling, 32, 04-15–04-16.

McFarquhar, G. M., and A. J. Heymsfield, 1997: Parameterization of tropical cirrus ice crystal size distribution and implications for radiative transfer: Results from CEPEX. J. Atmos. Sci., 54, 2187–2200.

Rotstayn, L. D., 1997: A physically based scheme for the treatment of clouds and precipitation in large-scale models. I: Description and evaluation of the microphysical processes. J. Roy. Meteor. Soc., 123, 1227–1282.

Sommeria, G., and J. W. Deardorff, 1977: Subgrid-scale condensation in models of non-precipitating clouds. J. Atmos. Sci., 34, 345–355.

A first version of the ice model for the global NWP system GME of the German Weather Service

Dmitrii Mironov and Bodo Ritter
German Weather Service, Offenbach am Main, Germany†

A first version of the ice model for the global numerical weather prediction system GME (cf. Majewski et al. 2002) of the German Weather Service (DWD) is developed. The model accounts for thermodynamic processes only (detailed descriptions of several dynamic-thermodynamic ice models and further references can be found at `http://stommel.tamu.edu/~baum/ocean_models.html`). A distinguishing feature of our model is the treatment of the heat transfer through the ice. Most currently used ice models carry the heat transfer equation that is solved on a finite difference grid where the number of grid points and the grid spacing differ with the application. We use the integral, or bulk, approach. It is based on a parametric representation of the evolving temperature profile within the ice that is conceptually similar to a parametric representation of the temperature profile in the seasonal thermocline in the ocean or lakes. The essence of the concept (Kitaigorodskii and Miropolsky 1970) is that the dimensionless temperature profile in the thermocline can be fairly accurately parameterized through a "universal" function of dimensionless depth, where the temperature difference across the thermocline and its thickness are used as the relevant scaling parameters. We use this concept to parameterize the temperature profile within the ice.

The ice thickness $H(t)$ and the temperature difference $T_s(t) - T_f(t)$ across the ice are utilised as appropriate scales of depth and temperature, respectively. Here, $T_s(t)$ is the temperature at the air-ice interface, and $T_f(t)$ is the temperature at the ice-water interface that is equal to the freezing point. Then, the temperature profile $T(z,t)$ within the ice is represented as $[T(z,t) - T_f(t)] \,/\, [T_s(t) - T_f(t)] = \Phi(\zeta)$, where Φ is a dimensionless universal function of dimensionless depth $\zeta = z/H(t)$ referred to as the "shape function". Notice that the assumption about the shape of the temperature profile within the ice is either explicit or implicit in many ice models developed to date. Using the above parameterization of the temperature profile, the heat transfer equation is integrated over z from the lower side to the upper side of the ice to yield the equation of heat budget of the ice layer. The evolution equation for the ice thickness is developed by considering the heat balance at the air-ice interface and at the ice-water interface. The result is the ice model that consists of two ordinary differential equations for the two time-dependent quantities, $T_s(t)$ and $H(t)$. Upon integration of the heat transfer equation over the ice layer the exact knowledge of the shape function is no longer required. It is not $\Phi(\zeta)$ per se, but the so-called shape factor $C_I = \int_0^1 \Phi(\zeta) d\zeta$ that enters the model equations. The shape factor may either be estimated independently, using empirical data on the temperature distribution within the ice, or be considered as adjustable tuning parameter. Its major effect is to control the thermal inertia of the ice layer.

The above ice model is implemented into GME and the test runs are performed, using $C_I = 1/2$ and a constant sea water freezing point $T_f = -1.7°\mathrm{C}$. The model is currently set up in a way that (i) the ice covers the entire GME grid box, and (ii) no ice is created in the GME grid box over the forecast period if this grid box has been set ice-free during the initialisation. As an example of the forecast sensitivity, Fig. 1 shows the surface pressure over Greenland and part of North Atlantic. Results with the new ice model show somewhat more structure in the pressure field, apparently as a result of the air-ice interaction. This

†Corresponding address: Deutscher Wetterdienst, Referat FE14, Frankfurter Str. 135, D-63067 Offenbach am Main, Germany. E-mail to Dmitrii.Mironov@dwd.de and Bodo.Ritter@dwd.de.

interaction is lacking in the operational GME ice model, where the ice surface temperature is set to a climatologically mean value and is kept constant over the forecast period.

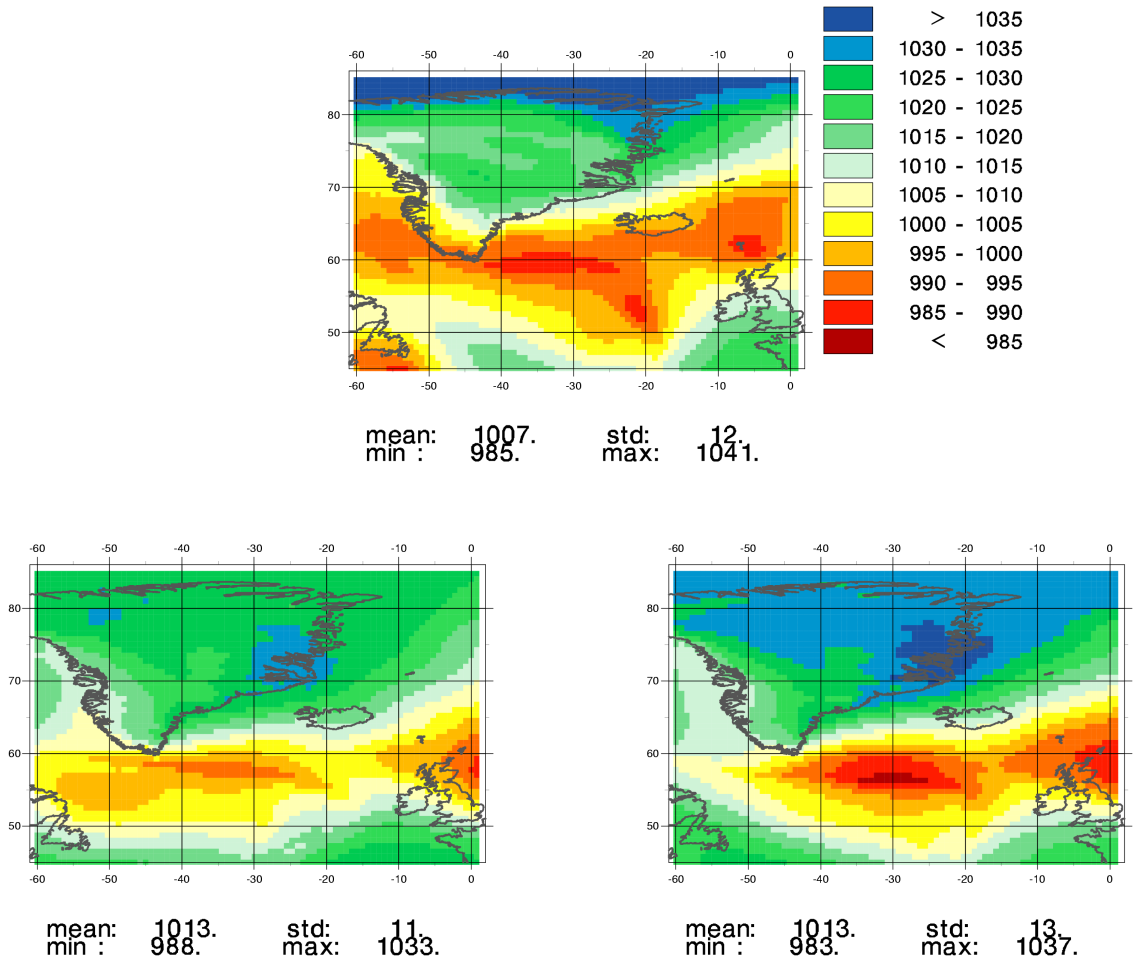

Figure 1. The 12 UTC 01.03.2003 GME analysis, upper panel, versus 168 h GME forecast of the surface pressure produced with the operational ice model, lower left panel, and the new ice model, lower right panel.

In the new model, provision is made to account for the snow layer over the ice. The snow is treated in the same way as the ice, i.e. through the use of a temperature-profile shape function and the integral heat budget of the snow layer.

Acknowledgements. The work was partially supported by the EU Commissions through the project INTAS-01-2132.

References

Kitaigorodskii, S. A., and Yu. Z. Miropolsky, 1970: On the theory of the open ocean active layer. *Izv. Akad. Nauk SSSR. Fizika Atmosfery i Okeana*, **6**, 178–188.

Majewski, D., D. Liermann, P. Prohl, B. Ritter, M. Buchhold, T. Hanisch, G. Paul, W. Wergen, and J. Baumgardner, 2002: Icosahedral-hexagonal gridpoint model GME: description and high-resolution tests. *Mon. Weather Rev.*, **130**, 319–338.

Numerical Simulations of a Tropical Cyclone using the Arakawa-Schubert Scheme with Vertically Variable Entrainment Rate

Akihiko MURATA and Mitsuru UENO

Meteorological Research Institute / Japan Meteorological Agency, Tsukuba, Ibaraki 305-0052, Japan
(corresponding author: amurata@mri-jma.go.jp)

1. Introduction

Numerical simulations for tropical cyclones provide an extremely useful test for the depth of knowledge about cumulus parameterization (Ueno, 2000). We therefore have investigated effects of some cumulus parameterizations on tropical cyclone simulations. As a consequence it was found that the Arakawa-Schubert scheme guaranteed relatively good performance (e.g., Murata and Ueno, 2000). It has been pointed out, however, that fractional entrainment profiles in the scheme did not agree with those of observations and numerical experiments. Lin (1999) investigated entrainment profiles using simulated data from a slab-symmetric cloud-resolving model. He found that entrainment for each cloud type, which was categorized in terms of cloud top height, tended to be significant near cloud base and cloud top.

In this study, on the basis of the results from the three-dimensional cloud-resolving model (CRM), vertically variable entrainment rate is applied to a version of the Arakawa-Schubert scheme. The impact of the modified scheme on the simulations of typhoon Saomai (2000) is investigated.

2. Estimate of entrainment rate with a cloud-resolving model

The Meteorological Research Institute / Numerical Prediction Division nonhydrostatic model (MRI/NPD-NHM; Saito et al., 2001) with 200 m horizontal resolution is used as CRM. The model includes bulk cloud microphysics by Ikawa et al. (1991), which predicts the mixing ratios of six water species (water vapor, cloud water, rain, cloud ice, snow and graupel) and the number concentration of cloud ice. A domain (280×280) is set on a spiral rainband of Saomai. A 20-min simulation is conducted by using a one-way nest with output from the 1-km grid MRI/NPD-NHM.

Before the calculation of entrainment rate, a cumulus area, where a single cumulus is contained, is extracted from the CRM output. The calculation is conducted on the basis of the definition, dM/Mdz, where M is mass flux averaged over cumulus grids and z is height. The cumulus grids are defined as those at which the sum of mixing ratios as to cloud water and cloud ice is larger than 0.1 g/kg and vertical velocity is positive.

The result of the calculation clearly shows high entrainment rate just above the cloud base and just below the cloud top. Figure 1 displays the characteristic entrainment profiles that have larger amounts between 1.0 and 1.5 km high and between 6.5 and 7.0 km high. The layers in between are marked by relatively low entrainment rate.

3. Experimental design

MRI/NPD-NHM with 20-km horizontal grid length is used in the simulations of Saomai. We incorporate a version of the Arakawa-Schubert (AS) scheme (Kuma et. al. 1993), which has the prognostic equation that predicts the cloud base mass flux and has a downdraft and a mid-level convection, into MRI/NPD-NHM.

A profile of entrainment rate, λ, in the AS scheme is modified so that they can qualitatively represent the feature revealed in the CRM result. The assumed profile is as follows:

$$\lambda = A\{1-\sin(\frac{2\Delta}{z_T - z_B} z + \frac{\pi}{2} - \frac{z_T + z_B}{z_T - z_B}\Delta)\} + S$$

$$A > 0, S > 0, \Delta < \pi / 2$$

where z_B and z_T are cloud base and top height, respectively. Among unknown constants, Δ is set at 5×10^{-3}. The remaining constants A and S are determined so that following two conditions are satisfied. One of them is that the cloud top level is located where buoyancy in the cloud disappears. The other condition is that the entrainment rate at the cloud base, λ_B, is determined on the basis of the CRM result, which indicates that λ_B falls within the range between the order of 10^{-3} to 10^{-2} m^{-1}. As for the AS scheme, λ ranges from the order of 10^{-4} to 10^{-3} m^{-1}. λ_B therefore is set at $\lambda_B = k\lambda$, where k is constant that controls the degree of the cloud-base entrainment rate. With k varying among 2, 3, 5 and 10 (referred as the experiments of AS2, AS3, AS5 and AS10, respectively), 36-hr integrations are conducted to examine the sensitivity of k.

4. Results of numerical experiments

Difference in the entrainment rate profile has drastic influence on simulated precipitation patterns. The axisymmetric eyewall is reproduced in AS5, whereas more scattered feature is shown in AS (Fig.2). The precipitation in the former tends to lie in the location relatively near the storm center. The radial profiles of accumulated rainfall amount are shown in Fig.3. From the figure, it is found that the rainfall amount over the outer area (outside the 200 km radius) decreases with increases in the entrainment rate (i.e., increases in k).

The radial distribution of precipitation seems to play a role in the size of the simulated tropical cyclone. The radial profiles of the axisymmetric tangential wind velocity change (Fig.4) clearly shows that the quantities over the outer area decrease with increasing the cloud-base entrainment rate, which is the same aspect as the precipitation. The result indicates that the storm grows as the entrainment rate drops.

The less rainfall over the outer area in the larger entrainment case is accounted for by relatively little mass flux calculated by the modified scheme. The vertical profiles of the cloud mass flux, averaged over the area ranging from 200 to 500 km radii, display that the mass flux is weaker in the larger entrainment cases (Fig.5), suggesting that vertical static instability in the outer area is not eliminated so much as those of the smaller entrainment cases.

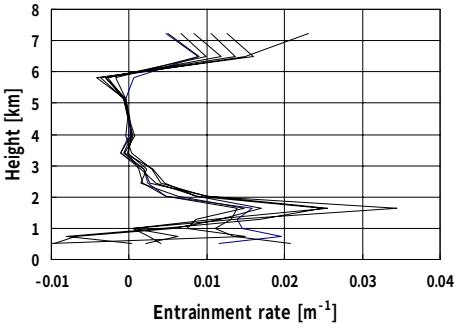

Fig.1 Vertical profiles of entrainment rate calculated by the CRM output. Lines are drawn every 5 sec from 6 min to 6 min 30 sec.

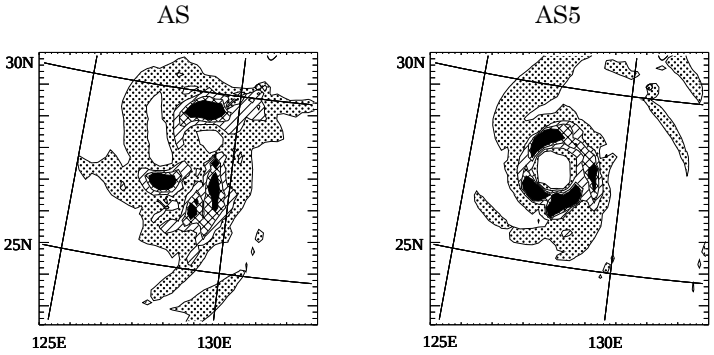

Fig.2 Horizontal distributions of 1-hr accumulated rainfall amount at 24 hr. Contours are drawn at 1, 5, 10 and 15 mm/hr.

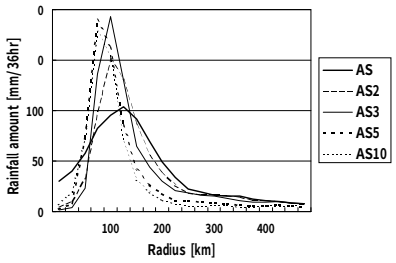

Fig.3 Radial profiles of azimuthally averaged 36-hr accumulated rainfall amount.

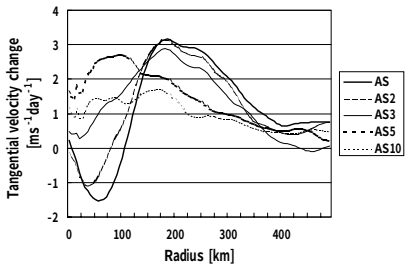

Fig.4 Radial profiles of azimuthally averaged tangential wind velocity change (between the initial and the end of the integration) on the surface. Unit is transformed to ms^{-1} day^{-1}.

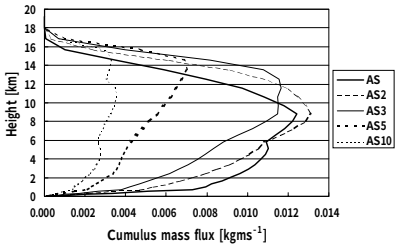

Fig.5 Vertical profiles of areally (200-500 km radii) and temporally (36 hr) averaged cumulus mass flux.

References

Ikawa, M., H. Mizuno, T. Matsuo, M. Murakami, Y. Yamada and K. Saito, 1991: Numerical modeling of the convective snow cloud over the Sea of Japan. -Precipitation mechanism and sensitivity to ice crystal nucleation rates-. J. Meteor. Soc. Japan, **69**, 641-667.

Kuma, K., C.-H. Cho, C. Muroi and M. Ueno, 1993: Improvement of typhoon track forecast by the JMA global model: An impact of cumulus parameterization. Papers presented at the third Technical Conference on SPECTRUM. Report No. TCP-33, WMO/TD-No. 595. World Meteor. Org., Geneva, Switzerland, Ⅳ 1-8.

Lin, C., 1999: Some bulk properties of cumulus ensembles by a cloud-resolving model. Part II: Entrainment profiles. J. Atmos. Sci., **56**, 3736-3748.

Murata, A. and M. Ueno, 2000: The Effects of different cumulus parameterization schemes on the intensity forecast of typhoon Flo (1990). J. Meteor. Soc. Japan, **78**, 819-833.

Saito, K., T. Kato, H. Eito and C. Muroi, 2001: Documentation of the Meteorological Research Institute / Numerical Prediction Division unified nonhydrostatic model. Tec. Rep. MRI, **42**, 133pp.

Ueno, M., 2000: Numerical prediction for tropical cyclones. Meteorology Research Note, **197**, 131-286 (in Japanese).

Development of a Cumulus Parameterization Scheme of the Operational Global Model at JMA

Masayuki Nakagawa
Numerical Prediction Division, Japan Meteorological Agency
1-3-4 Otemachi, Chiyoda-ku, Tokyo 100-8122, JAPAN
m-nakagawa@met.kishou.go.jp

The cumulus parameterization scheme implemented in the Japan Meteorological Agency (JMA) Global Spectral Model (GSM) follows the scheme proposed by Arakawa and Schubert (1974) with modifications by Moorthi and Suarez (1992), Randall and Pan (1993) and Pan and Randall (1998). JMA revised the cumulus parameterization scheme of operational GSM in March 2001 to include reevapolation effect of the convective precipitation (GSM0103). The aim of this revision is to improve performance in the medium- and long-range predictions of tropical precipitation and associated circulation. However, this revision produced a systematic negative error in temperature and geopotential height fields at lower troposphere over the western portion of the North Pacific high in early forecast days. The main reason for this error is the excessive cooling by the evaporation of convective precipitation. At the same time, it is known from a forecast experiment that the GSM can not maintain the atmospheric general circulation over a long period without cooling and moistening effects of the reevapolation.

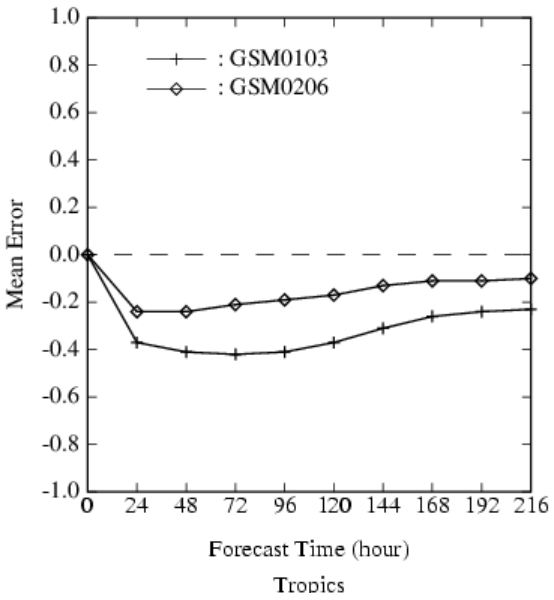

Fig. 1. Mean forecast error of 850 hPa temperature (K) over the tropics (20S-20N) averaged for the 15 cases. +: GSM0103, o: GSM0206.

JMA has been developing a new cumulus parameterization scheme which includes the entrainment and detrainment effects between the cloud top and the cloud base in convective downdraft instead of reevapolation of convective precipitation (GSM0206). To test the impact of the new scheme, two data assimilation experiments using GSM0103 and GSM0206 were conducted for the period 1-31 July 2001. Nine days forecasts were performed for 15 cases starting from 12UTC 8-22 July 2001. The results were compared with each other.

Figure 1 shows the mean forecast error of 850 hPa temperature over the tropics (20S-20N) averaged for the 15 cases with respect to the forecast time. It is seen that

the GSM0103 forecast shows systematic negative bias throughout the forecast period up to -0.42 K. The bias of the GSM0206 forecast is about half as much as that of the GSM0103 forecast. This difference is caused by the change of the cumulus parameterization scheme. Root mean square errors for the both experiments were also calculated and found to be comparable (not shown).

The 24-hour forecast and its mean error for 500 hPa geopotential height field are shown in Fig. 2. The field simulated by GSM0103 is systematically lower than the analysis field in wide area extending from the North Pacific high to the Asian monsoon region. GSM0206 makes much better forecast than GSM0103 due to the smaller temperature bias at lower troposphere.

In conclusion, the new cumulus parameterization scheme suppresses the systematic errors of GSM0103 in temperature and geopotential height fields at lower troposphere. JMA plans to implement this scheme in operational GSM in April 2003.

References.

Arakawa, A. and W. H. Schubert, 1974: Interaction of a cumulus cloud ensemble with the large-scale environment, Part I. *J. Atmos. Sci.*, **31**, 674-701.

Moorthi, S. and M. J. Suarez, 1992: Relaxed Arakawa-Schubert: A parameterization of moist convection for general circulation models. *Mon. Wea. Rev.*, **120**, 978-1002.

Pan, D.-M. and D. Randall, 1998: A cumulus parameterization with a prognostic closure. *Quart. J. Roy. Meteor. Soc.*, **124**, 949-981.

Randall, D. and D.-M. Pan, 1993: Implementation of the Arakawa-Schubert cumulus parameterization with a prognostic closure. Meteorological Monograph/The representation of cumulus convection in numerical models. *J. Atmos. Sci.*, **46**, 137-144.

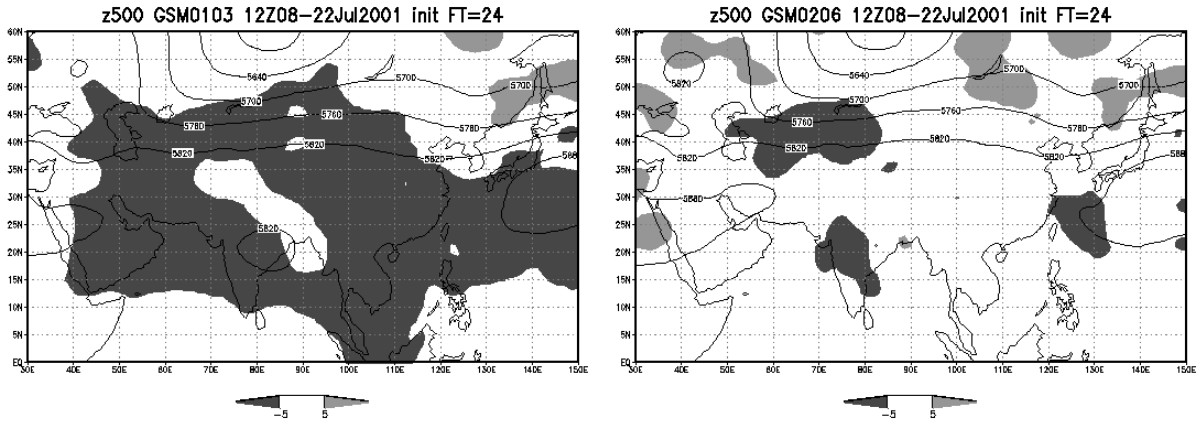

Fig. 2. Twenty four-hour forecast (contour) and mean forecast error (shade) of 500 hPa geopotential height (m) averaged for the 15 cases by GSM0103 (left) and GSM0206 (right). The contour interval is 60 m. Areas with mean forecast errors larger than 5 m are shaded.

Implementation of the NCAR Community Land Model (CLM) in the NASA/NCAR Finite-Volume Global Climate Model (fvGCM)

Jon Radakovich[1], Guiling Wanf, Shian-Jiann Lin, Sharon Nebuda and Bo-wen Shen

1. INTRODUCTION

In this study, the recently developed stateof- of-the-art NCAR Community Land Model (CLM) version 2.0 land-surface model (Dai et al. 2002; Zeng et al. 2002) was integrated into theNASA/NCAR finite-volume Global Climate Model(fvGCM; Lin and Rood 2002). The CLM2 provides a comprehensive physical representation of soil/snow hydrology and thermal dynamics and biogeophysics. The CLM2 was developed collaboratively by an open interagency/university group of scientists, and based on well-proven physical parameterizations and numerical schemes that combine the best features of three previous land surface models: Biosphere-Atmosphere Transfer Scheme (BATS; Dickinson et al. 1993), the NCAR Land-surface Model (LSM; Bonan 1996), and the IAP94 snow model (Dai and Zeng 1996). The Data Assimilation Office (DAO) has collaborated with NCAR to produce the NASA/NCAR fvGCM, which is a unified climate, numerical weather prediction, and chemistrytransport model suitable for data assimilation, with the DAO's finite-volume dynamical core and NCAR's suite of physical parameterizations.

2. RESULTS

The fvGCM coupled CLM2 was run at 2 x 2.5° horizontal resolution with 55 vertical levels for a 15-year period from 1991-2006 with initial conditions based on AMIP (Atmospheric Model Intercomparison Project) and fixed sea-surface temperatures based on an annual climatology. The 10-year climate from the fvGCM CLM2 Control run was then intercompared with the climate from fvGCM LSM, the European Center for Medium-range Weather Forecasting (ECMWF) reanalysis and the National Centers for Environmental Prediction (NCEP) reanalysis. We concluded that the incorporation of CLM2 did not significantly impact the fvGCM atmospheric climate circulation from that of LSM. The most striking difference was the warm bias in the CLM2 surface skin temperature over desert regions, which was equal and opposite to the LSM cold bias (Figure 1). We determined that the warm bias can be partially attributed to the value of the drag coefficient for the soil under the canopy (csoilc), which was too small for sparsely vegetated regions resulting in a decouplingbetween the ground surface and the canopy. We also found that the canopy interception was high compared to observations in the Amazon region. We performed several experiments designed to improve the CLM2 representation of surface hydrologic processes and the model's computational performance.

The experiments (Table 1), each of which included only one of the modifications, were run for 5 years starting in January 2000. All of the experiments were intercompared with the Control (the initial test case) based on a 2000-2004 average. The following experiments were completed: the exponential csoilc scheme (Experiment I), the leaf heat capacity scheme (Experiment II), the implicit leaf temperature scheme (Experiment III), the revised interception scheme (Experiment IV), the revised interception with sub-surface runoff turned off (Experiment V), and an experiment including all of the modifications (Experiment VI).

For Experiment I, csoilc was considered a function of vegetation density as represented by the LAI (Leaf Area Index), in order to correct the warm bias resulting from the decoupling. Analysis of the results revealed that there was a substantial impact, and the warm and dry bias in the fvGCM CLM2 was significantly reduced. The global annual mean bias and standard deviation for the intercomparisons of skin temperature with NCEP reanalysis presented in Figure 1, show a reduction in the standard deviation and the bias for Experiment I compared to the Control. Experiment II, the leaf heat capacity scheme, which was shown to improve the memory of skin temperature and impact its diurnal cycle, had only a marginal impact on the annual mean (Figure 1). Experiment III included changes to the numerical scheme that solves the water and energy balance of the vegetation canopy. An implicit scheme, which is scientifically accurate and computationally more efficient, replaced the explicit scheme previously used in CLM2 (Wang et al. 2002a). While the implicit scheme saves computation time, it does not cause noticeable changes in the model results (Figure 1)

For Experiment IV, the change involved incorporating precipitation sub-grid scale variability into the canopy interception scheme, which causes a decrease of interception loss and subsequent increase in the canopy throughfall (Wang et al. 2002b). The results from the 5-year run show that the new interception

[1] 1 *Corresponding Author Address*: Jon D. Radakovich, Science Applications International Corporation, Data Assimilation Office, NASA GSFC Code 910.3, Greenbelt, MD 20771, jrad@dao.gsfc.nasa.gov

run show that the new interception scheme causes about 0.5° in warming, which in turn increases the CLM2 warm bias when compared to NCEP (Figure 1). The positive impacts were an increase in the low-level moisture and a significant decrease in the interception loss ratio (canopy evaporation to precipitation). Experiment V included the modified interception scheme but with Z. -L. Yang and G. -Y. Niu's sub-surface runoff scheme turned off. This was done to correct some overestimation of lateral sub-surface runoff, which may have resulted from not considering the impact of topography in the runoff scheme. This produced a more realistic runoff ratio (runoff to precipitation). Inhibiting the sub-surface runoff also reduced the warming caused by the revised interception scheme (Experiment IV) and the results from Experiment V did not deviate much from the Control (Figure 1).

In Experiment VI, all of the modifications were incorporated and the largest and most beneficial change was attributed to the exponential csoilc scheme, which considerably decreased the warm bias in the CLM2 when compared to the Control. This result was expected based on Figure 1, which shows Experiment I having the most substantial impact. Also, the standard deviation from Experiment VI does not differ greatly from that of the fvGCM LSM (Figure 1).

Table 1: Description of experiments.

Experiment	Description
Control	Initial fvGCM CLM2 run
Experiment I	Exponential csoilc
Experiment II	Leaf heat capacity
Experiment III	Implicit leaf temperature
Experiment IV	Revised interception
Experiment V	Exp. IV w/o subsurface runoff
Experiment VI	All of the modifications (I-V)

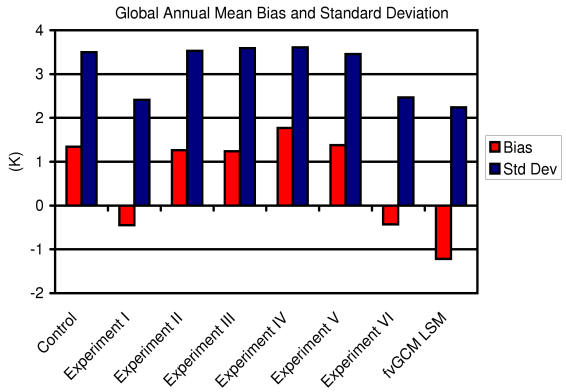

Figure 1. The global annual mean standard deviations of surface skin temperature between the Control, Experiments I-VI (Table I), and fvGCM LSM versus NCEP.

3. REFERENCES

Bonan, G. B., 1996: A land surface model (LSM version 1.0) for ecological, hydrological, and atmospheric studies. NCAR Tech. Note NCAR/TN-417+STR, 150 pp.

Dai, Y., X. Zeng, 1996: A land surface model (IAP94) for climate studies. Part I: Formulation and validation in off-line experiments. *Adv. Atmos. Sci.*, **14,** 433-460.

_____, and _____, R. E. Dickinson, I. Baker, G. Bonan, M. Bosilovich, S. Denning, P. Dirmeyer, P. Houser, G. Niu, K. Oleson, A. Schlosser, and Z.-L. Yang, 2002: The Common Land Model (CLM). (Submitted to *Bull. Amer. Meteor. Soc.*)

Dickinson, R. E., A. Henderson-Sellers, and P. J. Kennedy, 1993: Biosphere-Atmosphere Transfer Scheme (BATS) version 1e as coupled to the NCAR Community Climate Model. NCAR Tech. Note NCAR/TN-387+STR, 72 pp.

Lin, S.-J., and R. B. Rood 2002: A “vertically Lagrangian”finite-volume dynamical core for global models. (Submitted to *Mon. Wea. Rev.*)

Wang, G. L., M. G. Bosilovich, J. D. Radakovich, and P. R. Houser, 2002a: Incorporating the implicit scheme for vegetation water and energy balances into the coupled fvGCM CLM2. Presented to the Land Working Group at the CCSM Workshop, Breckenridge, CO.

_____, _____, _____, and _____, 2002b: A precipitation interception scheme for CLM2: considering the impact of sub-grid variability. Presented to the Land Working Group at the CCSM Workshop, Breckenridge, CO.

Zeng, X., M. Shaikh, Y. Dai, R. E. Dickinson, and R. Myneni, 2002: Coupling of the Common Land Model to the NCAR Community Land Model. *J. Climate*, **15,** 1832-1854.

Implementation and testing of a multi-layer soil model in the NWP models of DWD

Bodo Ritter, Reinhold Schrodin, Erdmann Heise, Martin Lange and Aurelia Mueller
Deutscher Wetterdienst, Research and Development
PO-Box 100465, 63004 Offenbach, Germany
E-mail: Bodo.Ritter@dwd.de

A multi-layer soil model, originally developed for the high resolution limited area model LM of DWD has been implemented in the global forecast model of DWD. The model comprises 7 active soil layers ranging in thickness from 1 cm close to the surface to roughly 5 m for the lowest layer. Below the active soil layers a climate layer with prescribed annual mean temperatures provides boundary conditions for the thermal heat flux computations. The hydrological part of the soil model operates on the same vertical grid and a partial or total freezing of soil water is accounted for in all layers (cf. Heise and Schrodin, 2002).

Since the scheme differs considerably from the currently operational 2 layer scheme, it has to be tested and validated thouroughly before operational implementation, which is scheduled for autumn 2003. This validation exercise included a participation in the ELDAS RhoneAGG model intercomparison experiment (cf. Boone et al., 2001). In the course of this exercise it was revealed that snow melting processes, which were based on the same single snow layer formulation as the previously soil scheme of DWD, were not simulated with sufficient accuracy. The problems were caused by an overestimation of snow density and the fact that ageing of the snow layer with a corresponding decrease of the snow surface albedo for solar radiation was not considered in the original formulation. Adjustment of the snow density to more realistic values and the introduction of an empirical formulation describing the ageing of snow as a function of time since the last significant snow fall solved this problem.

A one year integration based on initial data from January 1st 2002 of the full forecast model was performed in order to study potential bias problems in the evolution of the the soil layers, if, in contrast to the RhoneAGG experiment, where the forcing was prescribed, the soil scheme is forced by upper boundary fluxes provided by the atmospheric model. Since data assimilation schemes in operational NWP models introduce very little information directly into the soil scheme, it is essential that the soil model shows as little drift as possible with regard to prognostic variables. However, since a few W/m**2 imbalance in annual mean surface fluxes is sufficient to cause substantial deviations in the subsoil temperatures from their climatological mean values, the evolution of prognostic soil temperatures and water content, at least for high latitudes, is rather sensitive to the empirial relation describing the snow ageing. This demonstrates the need for a careful tuning of the free parameters of the soil model and a thorough validation of the scheme itself. It also supports the specification of a climatological lower boundary condition rather than a zero-flux condition.

As an example from this integration Fig.1 compares the simulated global distribution of snow for

the end of the first month of the integration and the same month in the following year. The good overall agreement is an indicator of a realistic simulation of the evolution of the snow distribution in the course of one year.

Further tests, in particular with regard to the comparison of the new versus the old scheme in operational forecasts and data assimilation will be performed in the near future.

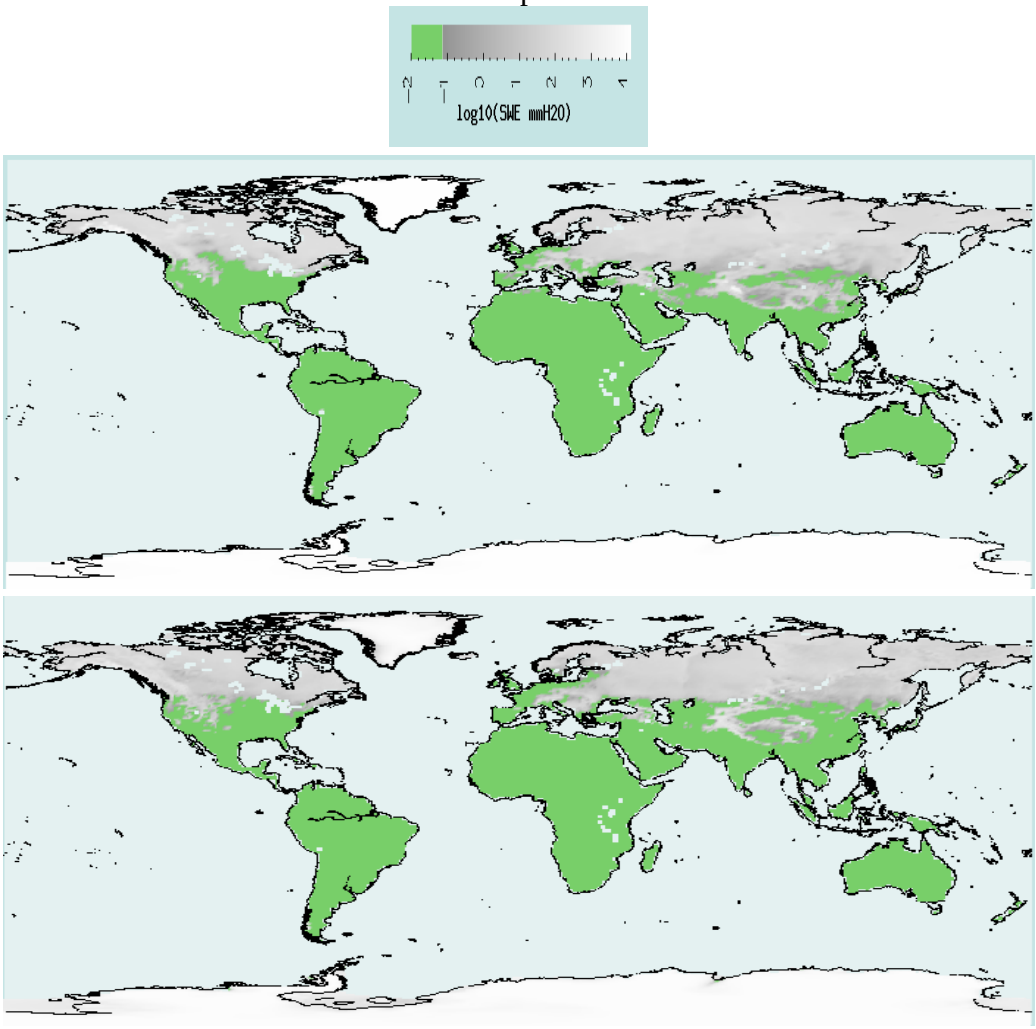

Fig.1: Simulated snow water content at end of first month (top) and one year further (bottom)

References

Boone, A., F.Habets and J.Noilhan, 2001: The Rhone-AGGregation Experiment. GEWEX News, WCRP, 11(3),3-5.

Heise, E. and R.Schrodin, 2002: Aspects of snow and soil modelling in the operational short range weather prediction models of the German Weather Service. Journal of Computational Technologies, Vo.7, Special Issue: Proceedings of the International Conference on Modelling, Databases and Information Systems for Atmospheric Science (MODAS), Irkutsk, Russia, June 25-29, 2001, 121-140

Implementation of ARM derived ice water content in NWP model

Z. Sun and L. Rikus
Bureau of Meteorology Research Centre, Australia
GPO BOX 1289K,Melbourne, VIC. 3001, Australia.
e-mail: Z.Sun@bom.gov.au

A cloud validating scheme was developed and has been running operationally at the Bureau of Meteorology since the early 90s (Rikus, 1997). This scheme uses physical parameterizations identical to those used in the Bureau of Meteorology Global Assimilation and Prediction System (GASP) and the forecast fields from GASP to generate narrow band brightness temperatures corresponding to a number of spectral infrared channels of geostationary satellites (e.g. GMS). The model cloud and radiation schemes are then validated by comparison of the modelled brightness temperature with the real satellite imagery.

One particular problem in the GASP system identified with this scheme is that the GASP model does not produce enough cold brightness temperatures in the tropics; the satellite image shows an appreciable percentage of brightness temperature below 200K whilst the minimum model brightness temperatures are only around 220K. After a series investigation the problem is found to be due to the ice water content diagnosed from the cloud temperature which is too low at the cold cloud temperature region. The implementation of a new diagnostic scheme proposed by Wang and Sassen (2002) based on the ARM lidar observation leads to a significant improvement in the model simulations.

Figure 1a-b shows a comparison between the modelled brightness temperature and measurements from GMS5 satellite imagery on 6 June 2002. The model generally captures the major characteristics of the brightness temperature distribution pattern observed by the satellite. But the modelled temperature is not cold enough compared with satellite results, especially over the tropical region. The minimum brightness temperature observed by the satellite is 193K but the modelled minimum value is only 222K. The difference is 29K. We have examined four other ice cloud optical property schemes and found that for the maximum ice water content used in the calculations the maximum difference in brightness temperature due to using different scheme is 8K, not big enough to explain the discrepancy between modelled results and observations.

Recently, Wang and Sassen (2002) presented a new relationship between ice water content and temperature determined from 4 years (1997-2000) of lidar-radar observations collected at the Southern Great Plains, at the site of the cloud and radiation testbed of Atmospheric Radiation Measurement (ARM) program in Oklahoma. They compared their results with aircraft observations taken over the mid-latitudes and found that the ice water content derived from the aircraft observations is higher for warm ice clouds ($T > -35^{o}C$) and lower for cold ice clouds ($T < -40^{o}C$). Figure 1c shows the relationship between ice water content and temperature determined using our scheme (solid curve) and that determined by Wang and Sassen (dotted curve). The symbols represent the aircraft observations to which the solid curve was fitted. The brightness temperature determined with the ARM scheme is shown in figure 1d. Clearly, the improvement from these changes is significant. This can be seen from the clouds over the tropics which are brighter than those shown in figure 1b. The other clear evidence is the modelled minimum brightness temperature which drops from 222K to 208K. This improvement indicates that the ice water content at cold temperatures in the GASP system is too small; it also raises a question on

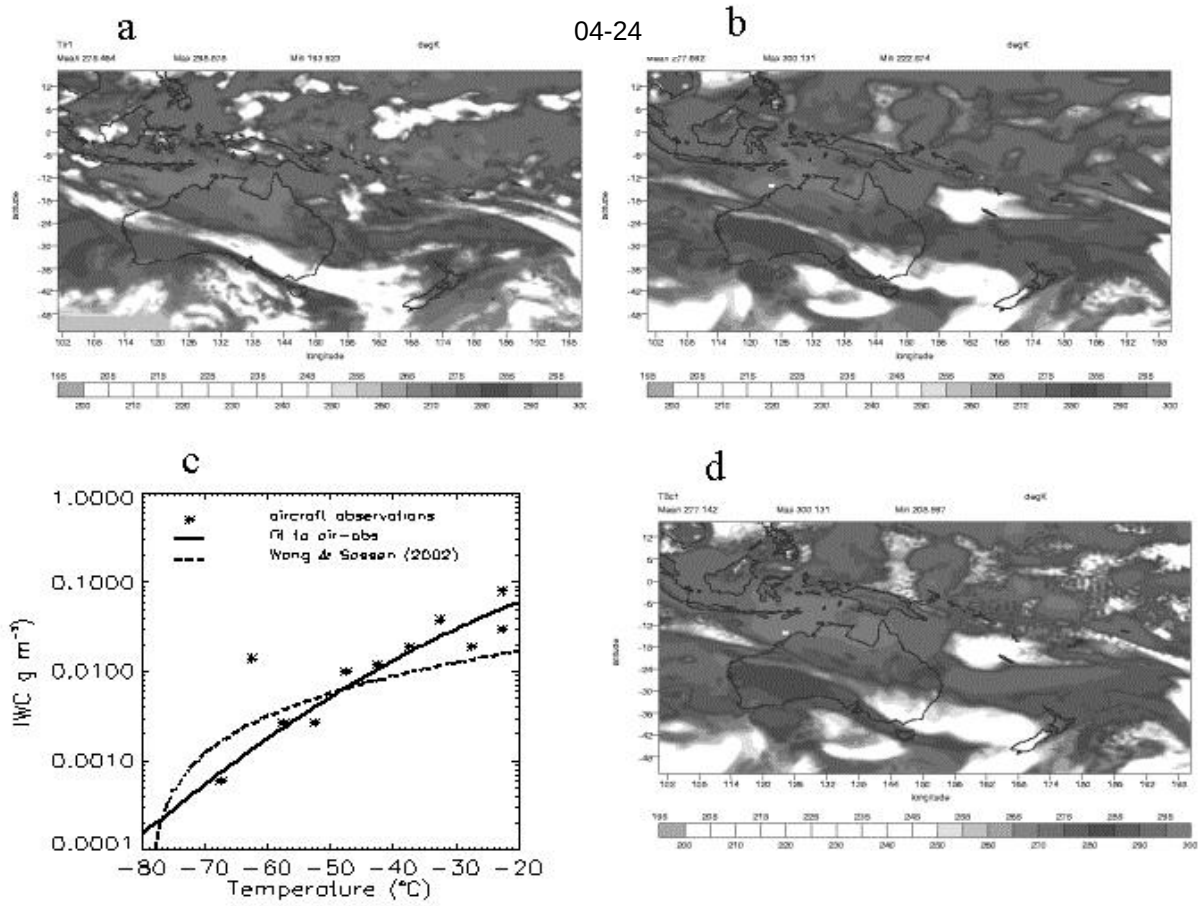

Figure 1: Panel a shows the brightness temperature from GMS5 satellite on 6 June 2002. Panel b is the modelled results using the original GASP ice water content scheme. Panel d is the same as panel b but using the Wang and Sassen ice water content scheme. panel c presents the ice water content as a function of cloud temperature determined using both the GASP scheme based on aircraft observation (solid curve) and Wang and Sassen scheme (dashed curve). The symbols in panel c represents aircraft observations.

the accuracy of ice water content measurements from aircraft at cold temperature region as the diagnostic ice water content scheme used in the GASP model is based on aircraft measurements.

REFERENCES

Rikus, L., Application of a scheme for validating cloud in an operational global NWP model, *Mon. Wea. Rev., 125,* 1615-1637, 1997.

Wang, Z., and K. Sassen, Cirrus cloud microphysical property retrieval using lidar and radar measurements. Part II: Midlatitude cirrus microphysical and radiative properties, *J. Atm. Sci., 59,* 2291-2302, 2002.

The use of combined closure in convection parameterization scheme

Mikhail Tolstykh

Institute of Numerical Mathematics, Russian Academy of Sciences,
and Russian Hydrometeorological Research Center
9/13 B. Predtecenskii per., 123242 Moscow RUSSIA

email:tolstykh@rhmc.mecom.ru

The SL-AV is a global semi-Lagrangian NWP model with variable resolution as an option [1]. The model includes the parameterization package of subgrid-scale processes from the French operational model ARPEGE/IFS [2]. The deep convection scheme is based on [3] but includes numerous developments (parameterization of dowdraught fluxes, redistribution of momentum, etc). Currently the resolution of the model is 1.40625x1.125 degrees lon/lat, and 28 vertical levels. It was found that for this (and coarser) resolution, the Kuo closure for deep convection parameterization works well in midlatitudes, while the closure based on CAPE (convective available potential energy) is better suited for tropics.

It is proposed to use a combination of these two closures, depending on average temperature near the surface. This idea was tested in the framework of the SL-AV model. The temperature which activates CAPE closure instead of Kuo closure is chosen to be 302.1 K. Obviously, this threshold can be used for tuning the parameterization.

On Fig. 1 we present zonal mean temperature trend averaged over 12 five-day forecasts starting from 15th of each month 1996, 0000 UTC (ECMWF data) for each type of closure and for combined closure. One can see that the use of combined closure reduces cold bias in upper troposphere in tropics with respect to "pure Kuo" case, but does not produces excessive warm bias near the surface, as "pure CAPE" does. There is also a small improvement in RMS scores for combined closure.

References

[1] M.A. Tolstykh, Semi-Lagrangian high resolution model of the atmosphere for numerical weather prediction, *Russian Meteorology and Hydrology*, N4, 1-9 (2001). (Russian and English)

[2] J.-F. Geleyn, E. Bazile, P. Bougeault *et al*, Atmospheric parameterization schemes in Meteo-France's ARPEGE N.W.P. model. In *Parameterization of subgrid-scale physical processes*, ECMWF Seminar proceedings (1994), 385-402.

[3] P. Bougeault, A simple parameterization of the large-scale effects of cumulus convection, *Mon. Wea. Rev.* **113** 2108-2121 (1985).

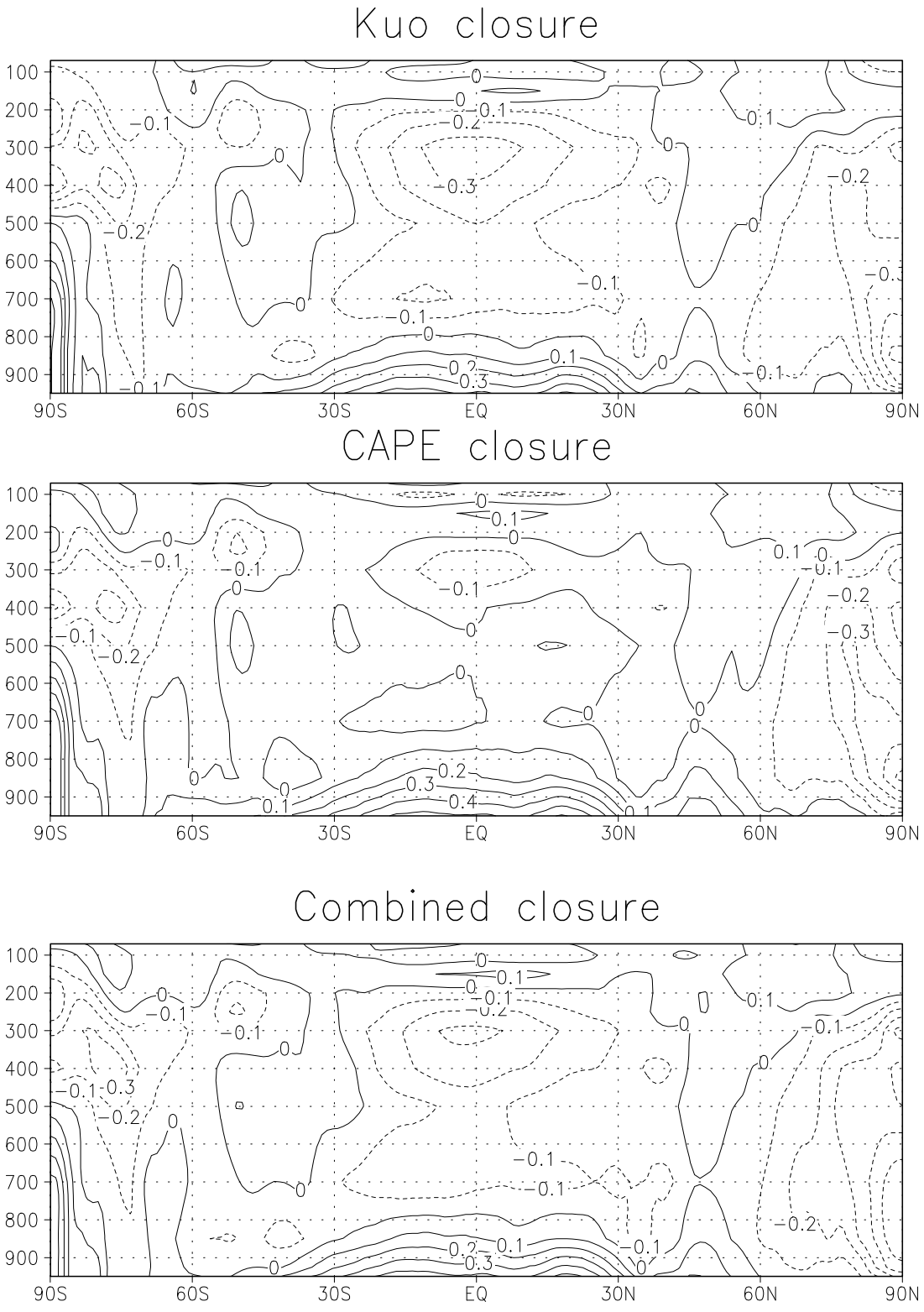

Рис. 1: The zonal mean temperature tendencies averaged over 12 cases for different closures (K/day)

An objective method to diagnose the contribution of steering flow at each level to tropical cyclone motion

Mitsuru Ueno
Typhoon Research Department, Meteorological Research Institute
e-mail: mueno@mri-jma.go.jp

Tropical cyclone (TC) motion is one of the most important forecasting issues both in the numerical weather prediction (NWP) and operational forecasting. Even with the state-of-the-art NWP models significant disagreements can be sometimes observed in TC track forecast among them although it has been believed that TC movement is primarily determined by the large-scale flow field and therefore should be well predicted with such models. A number of numerical studies demonstrate that the evolution of TC vortices is highly sensitive to the formulation of convective heating. So in this study our primary concern lies in (1) how significantly the environmental flow fields are affected by the formulation of convective heating, (2) whether or not asymmetric convective heating directly and significantly drives the TC vortices, and (3) how much the difference in vortex structure is responsible for the track difference.

In order to clarify the role of convective heating in TC motion, we conducted an idealized experiments using an f-plane version of a numerical prediction model, in which a tropical cyclone is embedded in a vertically sheared environment. A wide variety of TC motion shows up in the presence of the vertical shear, depending upon the formulation of convective heating (Ueno 2000). A preliminary analysis of the experimental results suggests that the difference not only in the steering flow but also in the axisymmetric structure of simulated TCs is responsible for the diversity of simulated TC motions. The latter's contribution can be defined by a set of weighting factors (referred to as steering weight) which is mathematically derived from surface pressure tendency equation and reflects upon the thermal structure of the individual vortex. Letting the steering weight at k-th model layer W_k and the steering flow at the same layer $\mathbf{v}_k$, the steering component of three-dimensional TC motion $\mathbf{v}_{STR}$ may be expressed as

$$\mathbf{v}_{STR} = \sum_{k=1}^{k\max} w_k \mathbf{v}_k \Delta\sigma_k \ , \ \Delta\sigma_k \equiv \Delta p_k / p_{srf}$$

where Δp_k is thickness in pressure of k-th model layer and p_{srf} is pressure at the sea surface. Figure 1 shows the vertical profile of the steering weight averaged over the integration period of 72 hours for two extreme track cases in Fig.1 of Ueno (2000), that is, B&M (experiment with Betts and Miller scheme) and KUR (experiment with Kurihara scheme). The profiles seem reasonable in that the weight is very small at the highest two layers near the tropopause, which is consistent with previous observational studies. Note that the two profiles significantly differ each other in the troposphere. Once we get the steering weight W_k, the steering motion component $\mathbf{v}_{STR}$ is easily computed using the steering flow $\mathbf{v}_k$ which is defined as an areal-mean asymmetric flow near the storm center. Figure 2 compares the track reproduced from hourly $\mathbf{v}_{STR}$ with "actual" one which is obtained as successive MSLP center locations. To see the impact of steering weight on the reproduced track, the tracks obtained by using mismatched steering weight (i.e., KUR-weight for B&M and B&M-weight for KUR) are shown in the same figure. The result demonstrates that the long-term vortex motion is well reproduced by the proper combination of the steering weight and steering flow. An additional experiment shows that the

steering weight is somewhat inherent to the convection scheme used and robust against the change of environment. Details of the discussions may be found in Ueno (2002).

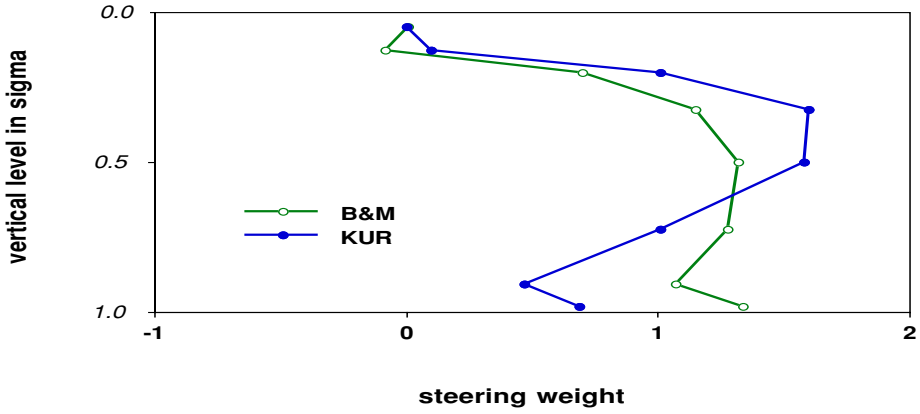

Figure 1: Vertical profile of steering weight. Symbols are put at each model level.

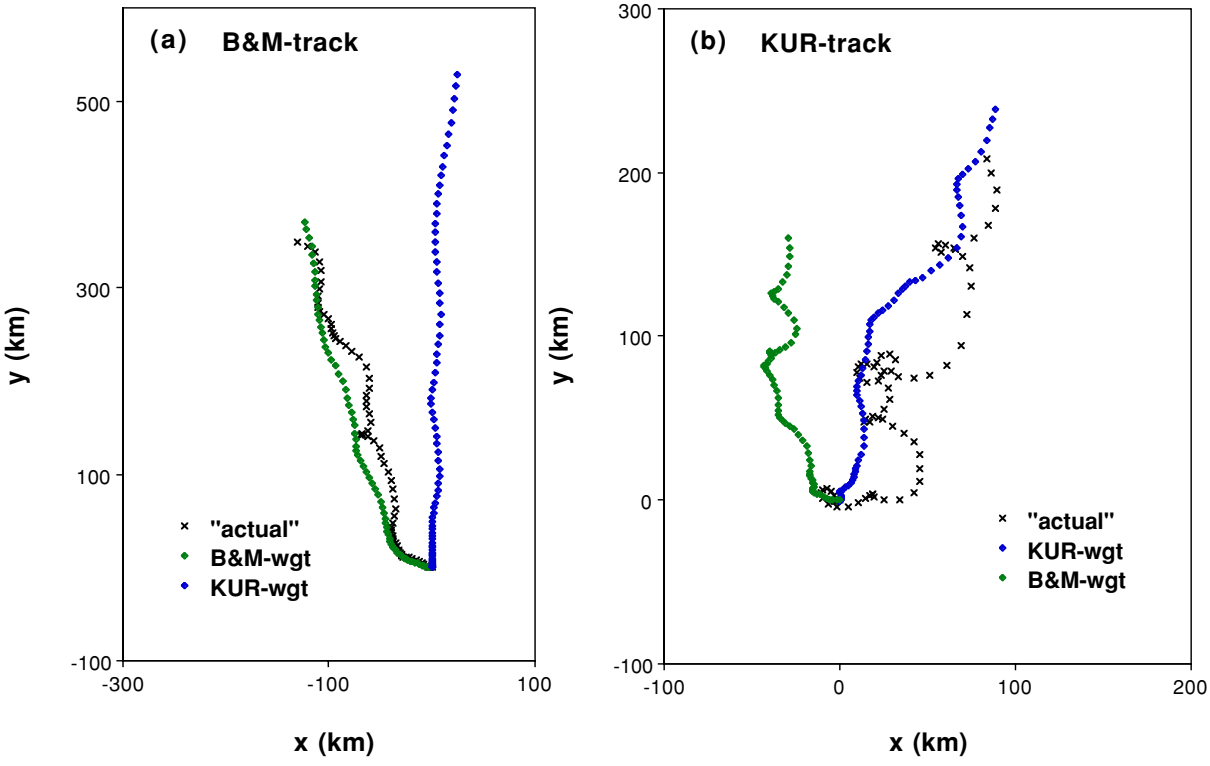

Figure 2: Vortex tracks reproduced from velocity components for (a) B&M and (b) KUR. The vortex is placed at (0,0) initially and symbols indicate hourly positions up to 72 h.

References

Ueno, M., 2000: Impact of upper-level flow on the tropical cyclone motion in a vertically sheared ambient flow. *WMO/TD-No.987*, 5.39-40.

Ueno, M., 2002: Steering weight concept and its application to tropical cyclones simulated in a vertical shear experiment. Submitted to *J. Meteor. Soc. Japan*.

The Doppler Absorption in the Thermal Infrared Radiation Parameterization of JMA Global Spectrum Model

Syoukichi Yabu
Japan Meteorological Agency, Tokyo, Japan
(email address: yabu@met.kishou.go.jp)

In longwave(LW) radiation scheme of the atmospheric numerical model, the stratosphere and the troposphere cannot be treated in the same manner. As an altitude becomes higher in the stratosphere, the dominant absorption line profile changes from a Lorentz line shape(collisional broadening) to a Doppler line shape(Doppler broadening). The operational global NWP model of Japan Meteorological Agency(JMA-GSM0103) does not sufficiently take account of the latter absorption type. The calculation method of the transmission function is based on the statistical band model(Goody,1952), where a Lorentz line shape is assumed. The Doppler effect is simply included by retaining a finite absorption under low pressure conditions where the pure Lorentz absorption would be normally negligible. GSM0103 has great error in temperature in the stratospheric region (shown later), and this insufficient treatment of the Doppler absorption in the LW radiation scheme is thought to be as one of its cause.

New parameterization is being developed in order to introduce the Doppler absorption properly. It is based on the LW radiation scheme of the NASA Goddard Space Flight Center (Chou et al.,2002) and the Doppler effect is considered by using the transmittance tables precomputed with the accutate line-by-line(LBL) culculation considering the Doppler broadening. Transmission of an atmospheric path can be calculated by reffering to these tables with an effective pressure and temperature computed by weighting the absorber amount along a path (2-parameter scaling method).

Cooling rates by LW radiation are computed by this new parameterization and the one used in GSM0103. Fig.1 and 2 respectively show the results for the mid-latitude summer and the tropical atmosphere taken from McClatchey et al.(1972), which are devided into 40-layers of GSM0103 in calculation. The figures indicate that (1) the cooling in the upper stratosphere is increased because of introducing the Doppler absorption properly, (2) the cooling in the middle stratosphere is decreased, and (3) the cooling in the troposphere is also improved in terms of better agreement with the LBL results. It is supposed that (2) is due to the increase of the upward flux in the stratosphere with the change in the troposphere((3)).

Next, this parameterization is examined by the one month forecast experiment using JMA's global model. Fig.3 shows the one month mean error in zonal-mean temperature in July 2001. The revised version is the same as the GSM0103 except for the parameterization of the Doppler effect in the LW radiation scheme. The great contrast between positive error(above the 3-hPa level) and negative error(below it) computed by the original GSM0103 is eliminated, and the magnitude of that negative error is reduced in the new version. This impact is consistent with the above-mentioned (1) and (2). While the error is increased in some regions of the troposphere by the reflection of the above (3), this implies the necessity to improve the other physical processes in the troposphere, including cloud-radiation interaction process.

References

Chou,M.D.,M.J.Suarez,X.Z.Liang and M.M.-H.Yan,2002: A thermal infrared radiation parameterization for atmospheric studies, Technical report series on global modeling and data assimilation Volume **19**,NASA Goddard space flight center.

Goody,R.M.,1952: A statistical model for water vapour absorption, Q.J.Roy.Met.Soc,**78**,165-169.

McClatchey,R.A.,R.W.Fenn,J.E.A.Selby,F.E.Volz and J.S.Garing,1972: Optical properties of the atmosphere, 3rd ed.,AFCRL Envirn.Res.Papers No.**411**,108pp.

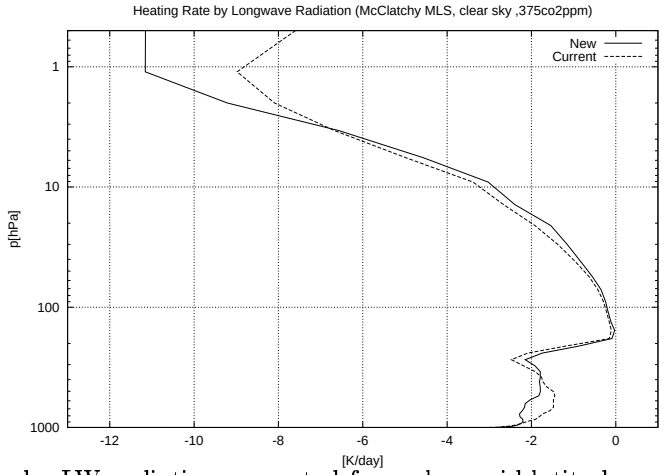

Fig.1: The heating rate by LW radiation computed for a clear mid-latitude summer atmosphere by the new parameterization(solid line) and the one used in GSM0103(dashed line)

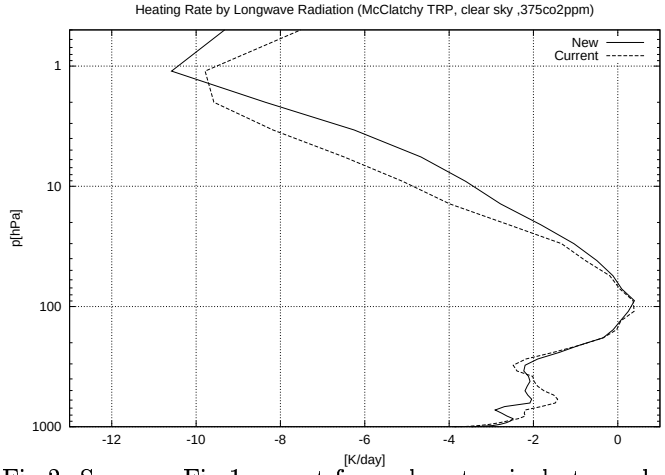

Fig.2: Same as Fig.1 except for a clear tropical atmosphere

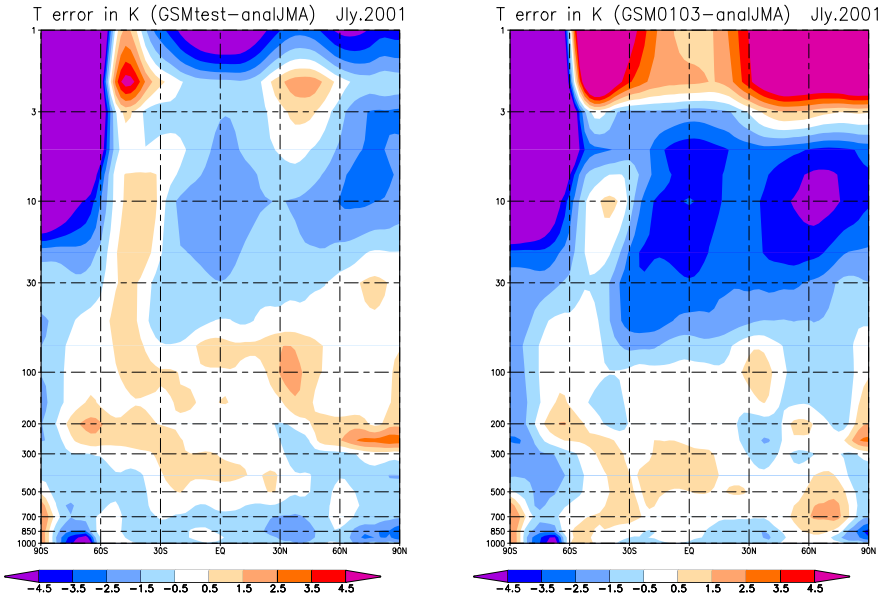

Fig.3: The one-month mean forecast error of zonal-mean temperature in July 2001. The current JMA-GSM0103(right) and the revised version using the new parameterization(left).